2006

Computational Modeling to Predict Mechanical Function of Joints: Validations and Applications of Lower Leg Simulations

Peter C. Liacouras
Virginia Commonwealth University

Computational Modeling to Predict Mechanical Function of Joints: Validations and Applications of Lower Leg Simulations

A dissertation submitted in partial fulfillment of the requirements for the degree of Doctor of Philosophy at Virginia Commonwealth University.

By

Peter Constantine Liacouras
B.S. James Madison University, 2000
M.S. Virginia Commonwealth University, 2002
Ph.D. Virginia Commonwealth University 2006

Director: Dr. Jennifer S. Wayne
Professor
Biomedical Engineering

Virginia Commonwealth University
Richmond, Virginia
August 2006

Acknowledgement

The author wishes to thank several people. I would like to thank my family for their love and support. I am especially grateful to Dr. Jennifer Wayne for giving me the opportunity to conduct research in the Orthopaedic Research Laboratory and for her help, guidance, and direction throughout this project. I appreciate all my colleagues, Johnny Owen, Kelly Shields, Karin Wartella, Joseph Iaquinto, and Justin Fisk, who extended their support and friendship over past several years. I would like to that Trimech Solutions, especially Tim Barker, for answering all my SolidWorks and COSMOSMotion questions. Finally I would like to thank the rest of the Orthopaedic Research Laboratory and all those in the School of Engineering for any assistance given to me during my time at VCU.

Table of Contents

List of Figures

List of Tables

List of Abbreviations

α	Angle of Rotation
ATFL	Anterior talofibular ligament
CFL	Calcaneofibular ligament
CT	Computed Tomography
cos	Cosine
cm	Centimeters
DICOM	Digital Imaging and Communications in Medicine
DVRT	Differential variable reluctance transducers
FEA	Finite Element Analysis
g/cm3	Grams per centimeter cubed
IGES	Initial Graphics Exchange Specification
in-lbf	Inch pounds of force
lb	Pound
lbf	Pounds of force
MIMICS	Materialise's Interactive Medical Imaging Control System
mm	Millimeters
MRI	Magnetic Resonance Imaging
N	Newtons

N/mm	Newtons per millimeter
N-mm	Newton millimeters
SIMM	Software for Interactive Musculoskeletal Modeling
sin	Sine
VIMS	Virtual Interactive Musculoskeletal System
3D	Three-dimensional
#	Number
%	Percent
±	Plus or minus

Abstract

COMPUTATIONAL MODELING TO PREDICT MECHANICAL FUNCTION OF JOINTS: VALIDATIONS AND APPLICATIONS OF LOWER LEG SIMULATIONS

By Peter Constantine Liacouras, Ph.D.

A dissertation submitted in partial fulfillment of the requirements for the degree of Doctor of Philosophy at Virginia Commonwealth University.

Virginia Commonwealth University, 2006

Major Director: Dr. Jennifer S. Wayne, Ph.D.
Professor
Biomedical Engineering

Computational models of musculoskeletal joints and limbs can provide useful information about joint mechanics. Validated models can be used as a predictive device for understanding joint function and serve as a clinical tool for predicting the outcome of surgical procedures. A new computational modeling approach was developed for simulating joint kinematics that are dictated by bone/joint anatomy, ligamentous constraints, and applied loading.

Three-dimensional computational models of the lower leg were created. Model development involved generating three-dimensional surfaces from CT images, followed

by importing these surfaces into SolidWorks and COSMOSMotion. Through SolidWorks and COSMOSMotion, each bone surface was created into a solid object and positioned, necessary components added, and simulations executed. Three dimensional contacts inhibited intersection of the bones during motion. Ligaments were represented as linear springs. Model predictions were then validated by comparison to three different previously performed cadaver studies (syndesmotic injury study, inversion stability study, and mechanical laxity study) and one simultaneously performed cadaver study (anterior drawer test).

In the syndesmotic injury study, the relative motion between the tibia and fibula in intact, transected, and repaired states was measured under the application of an external rotation of the ankle. The inversion stability study focused on the elongation behavior of lateral ankle ligaments and inversion range of motion during the application of an applied load. The mechanical laxity study focused on differences in anterior/posterior and inversion/eversion movement in intact and transected states. Each computational simulation was placed under the same conditions as its respective cadaver study and revealed a capability to predict behaviors in each case. The syndesmotic injury model was able to predict tibial rotation, fibular rotation, and anterior/posterior displacement. In the inversion simulation, calcaneofibular ligament extension and angles of inversion compared well. The laxity study showed increases in anteroposter motion after the transactions of the ATFL and CFL; and diffenences in inversion after the

transaction of the CFL. The Anterior Drawer simulation produced similar ligament elongations and loads when compared to cadaver studies.

Overall, the computational models were able to predict joint kinematics of the lower leg with particular focus on the ankle complex. Additional parameters can be calculated through such models that are not easily obtained experimentally such as ligament forces, force transmission across joints, and three-dimensional movement of all bones.

CHAPTER 1: BACKGROUND INFORMATION

1.1 INTRODUCTION

Computational models of musculoskeletal joints and limbs can provide useful information about joint interactions, joint kinematics, spatial positioning of bones/appendages, muscle/ligament lengths, muscle forces and moments, joint contact pressures, range of motion predictions, etc. These validated models can also be used for simulation of injuries and repairs, effects of fractures/osteotomies, surgical reconstructive procedures, changes in joint angles, changes due to ligament lengthening/shortening or deficiencies, variations due to different tendon attachment sites, etc.

Two common approaches for the development of these biomechanical models are finite element analysis based and multibody kinematics based [1-14]. Investigators employ finite element modeling to calculate stresses and strains within the bones or at the interface between a joint replacement and a bone. Multibody modeling, which maintains and assumes rigidity of the bones, is mainly performed to study soft tissue injury. While finite element models have yielded much useful information, a primary advantage of multibody modeling is its "ability to solve for mechanics of large structures using highly efficient algorithms which can execute much faster than the continuum-based finite element analysis (FEA)." [12] This modeling approach has been applied to the upper and

lower extremities as well as to specific segments such as the knee and wrist/hand complex. Many of these multibody models depend on experimental measurements of bone movements, assumptions about joint degrees of freedom, and moments associated with muscle forces to guide the motion in the computational models [1-8]. Fewer models incorporate articulation geometry, ligaments, and other anatomical features to guide joint function. Often this is accomplished by coding of governing mechanics equations and solution algorithms into custom computer programs. For knee kinematics using rigid three-dimensional multiple bodies and springs to represent ligaments, Wismans et al. and Hirokawa performed studies using rigid surface contacts between the bones of the knee joint while Kwak et al. allowed a small amount of overlap to account for articular cartilage. [12-14]

Other software packages for developing computational models of joints and extremities exist in the literature. SIMM (Software for Interactive Musculoskeletal Modeling) has been used for a wide variety of studies including how muscle architecture and moment arms affect movements, simulating musculoskeletal surgery, estimating muscle and tendon lengths during gait, and dynamic simulations of joint replacements. [2, 6, 15, 16] Ligaments in SIMM, as in our model, must be added manually. The advantage our modeling approach may have is the addition of three-dimensional contacts, rather than assuming joint degrees of freedom, and ease of incorporating external loading conditions, which with SIMM would require the addition of SDFast. [2] VIMS (Virtual Interactive Musculoskeletal System) asserts to be a database of anatomical bone dimensions, connective tissues, material properties, joint system functions, and loading

conditions. This software has been used for studies involving the hip in daily activities and the shoulder during throwing activities. [17, 18] VIMS is not currently available to the public.

Custom-designed rigid, three dimensional multibody models have been useful in studying and analyzing the knee. [12-14] However, multibody models that do not restrict the degrees of freedom and/or the kinematics of the lower leg and ankle joints have not been developed. In addition, the approach taken in this study could reduce the need for the creation of new software to analyze these models. New patient specific finite element models, generated from CT scans, have been constructed to look at the contact stress between the tibia and talus during physiological rotations about chosen axes, not motion experimentally measured nor predicted by the models. [19]

More recent studies have focused on the mechanics and kinematics of the ankle through Stress MRI techniques or Dual-Orthogonal Fluoroscopic and MRI imaging techniques. These new methods can trace/track movement of bones during loading or in the gait cycle. Since the talus is generally inaccessible to outside tracking devices, this can provide information on the talocrural and subtalar joints individually, instead of looking at the ankle complex as a whole.[20, 21] Also, these techniques are capable of looking at ligaments' characteristics, such as length changes during gait.[22] They can also depict ankle kinematics during ligament damage, and after surgical procedures under loading conditions.[23]

A graphically-based computational modeling approach implemented through available software packages could potentially expand the power and functionality of joint

modeling for simulating joint kinematics dictated by bone/joint anatomy, ligamentous constraints, and applied loading conditions. This could reduce the need to develop custom software to simulate joint function and take advantage of existing powerful graphical interfaces. Such expanded models can then be used to determine the kinematics of the joint under specified loads, as well as ligament reaction forces, ligament strains, object translations/rotations, etc. Moreover, validated models have the potential to serve as clinical tools by predicting the effects of surgical procedures.

The computational modeling approach presented here is not meant to replace these other programs or models but create another method of joint modeling which can be compared to experimental and clinical studies and add to the general understanding of joint function. Also with the appropriate programs, this technique of modeling can be performed by any laboratory.

In this study, a new computational modeling approach was developed to simulate joint function in which the kinematics are dictated by bone/joint anatomy, ligamentous constraints, and applied loading (muscle and/or external forces). One of the major benefits to this technique of computational modeling is that all the resources and programs used to create the models are in the public domain or commercially available. First, to illustrate the application of the approach, computational models were developed for the lower leg. For validation, the models were compared to previously and simultaneously conducted cadaver experimental studies. The cadaver studies evaluated the effects of a syndesmotic injury (rupture of specific tibia/fibula ligaments that stabilize the ankle mortise) on the relative motion of the fibula and tibia, the effects of inversion of

the ankle following ligament transection, and changes in ankle laxity (anterior/posterior and inversion/eversion movement) following ligament transections. The applied loading and boundary conditions from the experimental studies were simulated in the computational models and joint kinematics compared.

1.2 ANKLE ANATOMY

The foot and ankle must be able to withstand the load of the human body and adapt to rapidly changing surfaces. These joints help to perform normal everyday gait and help maintain balance. The leg/foot/ankle complex incorporates many bones and joints all serving a specific purpose.

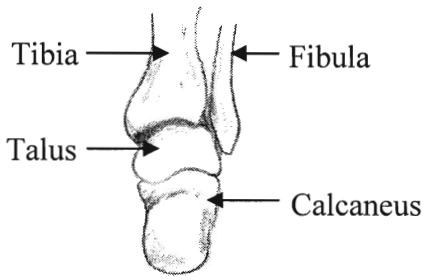

Figure 1.2.1: Articulations of the Foot/Ankle Complex: The four major articulations of the foot/ankle complex relevant to this study include: tibia/fibula, tibia/talus, fibula/talus, and talus/calcaneus. (picture redrawn and modified from [24])

The joints between the tibia and fibula are functionally classified as Amphiarthrotic, meaning they are slightly movable. Proximally, the tibiofibular joint is a plane synovial joint. The head of the fibula articulates with the posterolateral aspect of the tibia. The distal tibiofibular joint is a syndesmosis or a fibrous union. Distally, there

is no joint capsule. The primary purpose of the distal articulations is to stabilize the mortise and hold the talus in place. Between the proximal and distal articulation lies an interosseous membrane which is also a syndesmosis.[24-26]

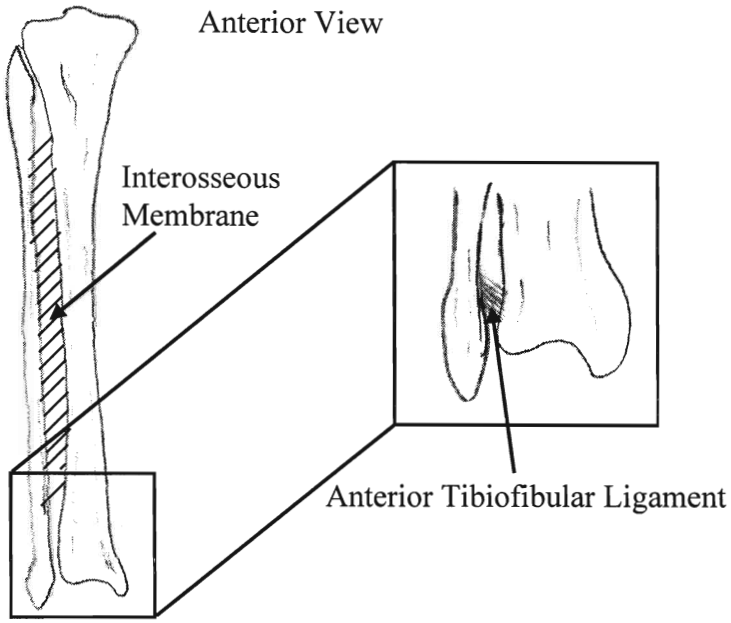

Figure 1.2.2: Proximal and Distal Tibia/Fibula Articulations: These articulations help to keep the tibia and fibula together. Anterior and posterior tibiofibular, both proximal and distal, ligaments as well as the interosseous membrane make this joint a slightly movable one. (picture redrawn and modified from [25])

The foot is a complex structure containing twenty-six bones. These bones include seven tarsal bones (talus, calcaneus, cuboid, navicular, and three cuneiforms), five metatarsals, and fourteen phalanges.

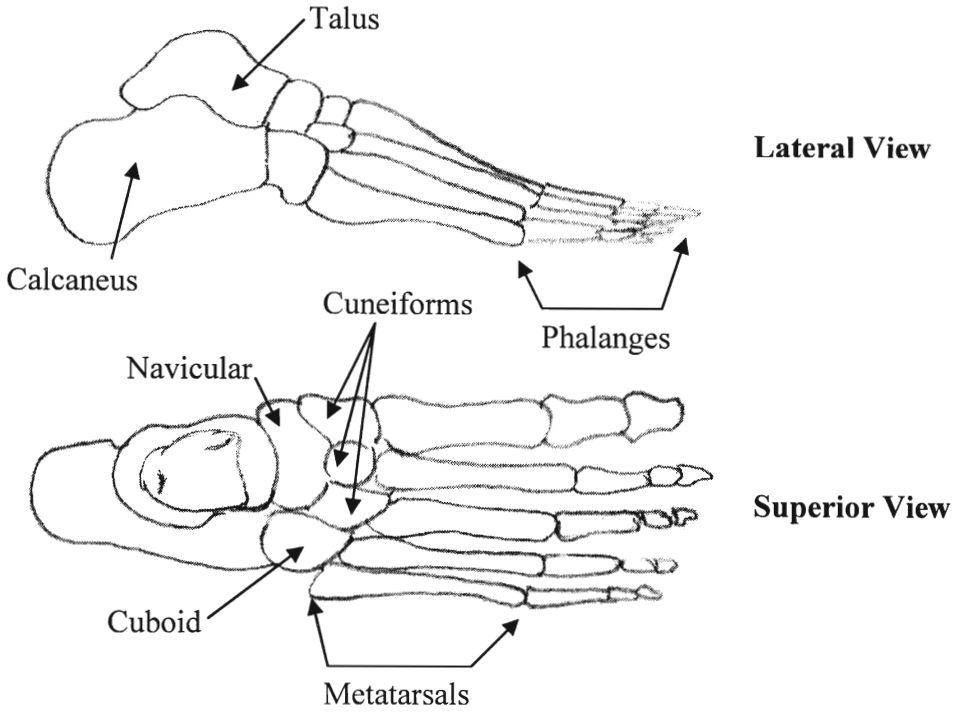

Figure 1.2.3: Bones of the Foot: The hindfoot is composed of the calcaneus and talus, the midfoot is composed of the navicular, cuboid and three cuneiforms, and the forefoot is composed of the metatarsals and phalanges. (picture redrawn and modified from [25])

The Ankle Joint generally refers to the talocrural joint. This joint incorporates the talus and the distal portions of both the tibia and fibula. The talocrural joint is structurally referred to as a synovial joint functioning as a hinge joint, having one degree of freedom, allowing plantar flexion and dorsiflexion (Figure 1.2.4) Some side to side motion does take place at this joint during plantar flexion. [24-26]

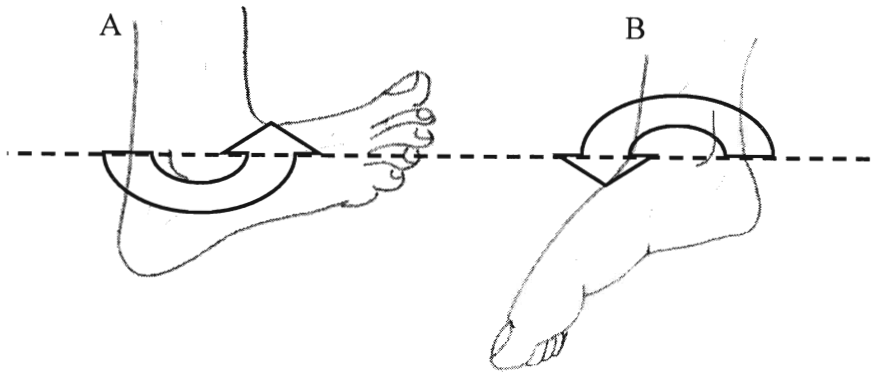

Figure 1.2.4: Movement of the Talocrural Joint: The talocrural joint is responsible for the movements of dorsiflexion and planter flexion. Dorsiflexion is defined as the turning of the foot or toes upward, while plantar flexion is defined as the movement of the foot that flexes the foot or toes downward toward the sole. Normal range of motion, from neutral, is approximately 20 degrees for dorsiflexion and anywhere from 30-50 degrees for plantar flexion.[25] (picture redrawn and modified from [24])

The Subtalar joint (talocalcaneal) and the transverse tarsal joints (talocalcaneonavicular and calcaneocuboid) allow the foot to adjust to tilted surfaces. The talus articulates with the calcaneus in three areas (posterior, middle, and anterior). The posterior articular surface of the talus is concave and the middle and anterior articular surfaces are convex These surfaces create a complex twisting motion at this joint along an oblique axis (inversion/eversion). The anterior head of the talus (ball) and the posterior aspect of the navicular along with the middle facets of the superior calcaneal surface (socket) makes what is considered structurally as a ball and socket joint.[25, 26]

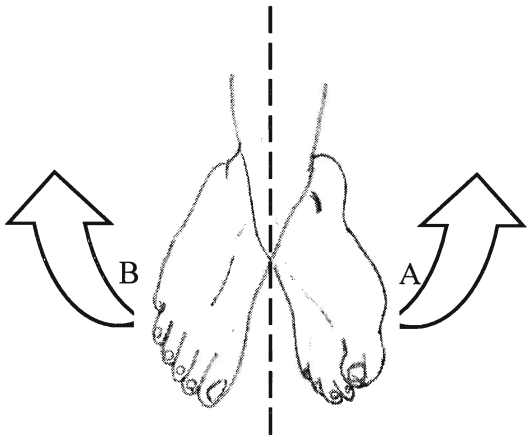

Figure 1.2.5: Inversion and Eversion: Inversion can be described as the as the foot rotating inward from the midline of the tibia toward the midline of the body (A). Eversion can be described as the as the foot rotating outward from the midline of the tibia away from the midline of the body (B). (picture redrawn and modified from [24])

The ankle is a load bearing joint that must be stable to produce proper gait. Inversion injuries of the ankle can lead to exaggerated movements within its joints. This movement beyond its normal physiological range is referred to as mechanical laxity.[27] Inversion stress is the most common cause of ankle injuries. The medial malleolus, being shorter than the lateral malleolus, allows more inversion than eversion, and the ligaments are separated unlike the medial side which make them easier to injure. [28] In Chapters 3-5 numerous cadaveric studies will be simulated which focused on several ligaments and the interosseous membrane that assist in the stability of the ankle joint complex.

CHAPTER 2: METHODS

2.1 OVERVIEW:

This computational model integrated both public domain and commercially available data sets and software. Joint anatomical features were obtained from separate male CT sets available from the National Library of Medicine's Visible Human Project. Detailed features of the foot/ankle complex were obtained by importing DICOM (Digital Imaging and Communications in Medicine) files of individual CT scans into MIMICS (Materialise's Interactive Medical Imaging Control System, Materialise, Ann Arbor, MI).

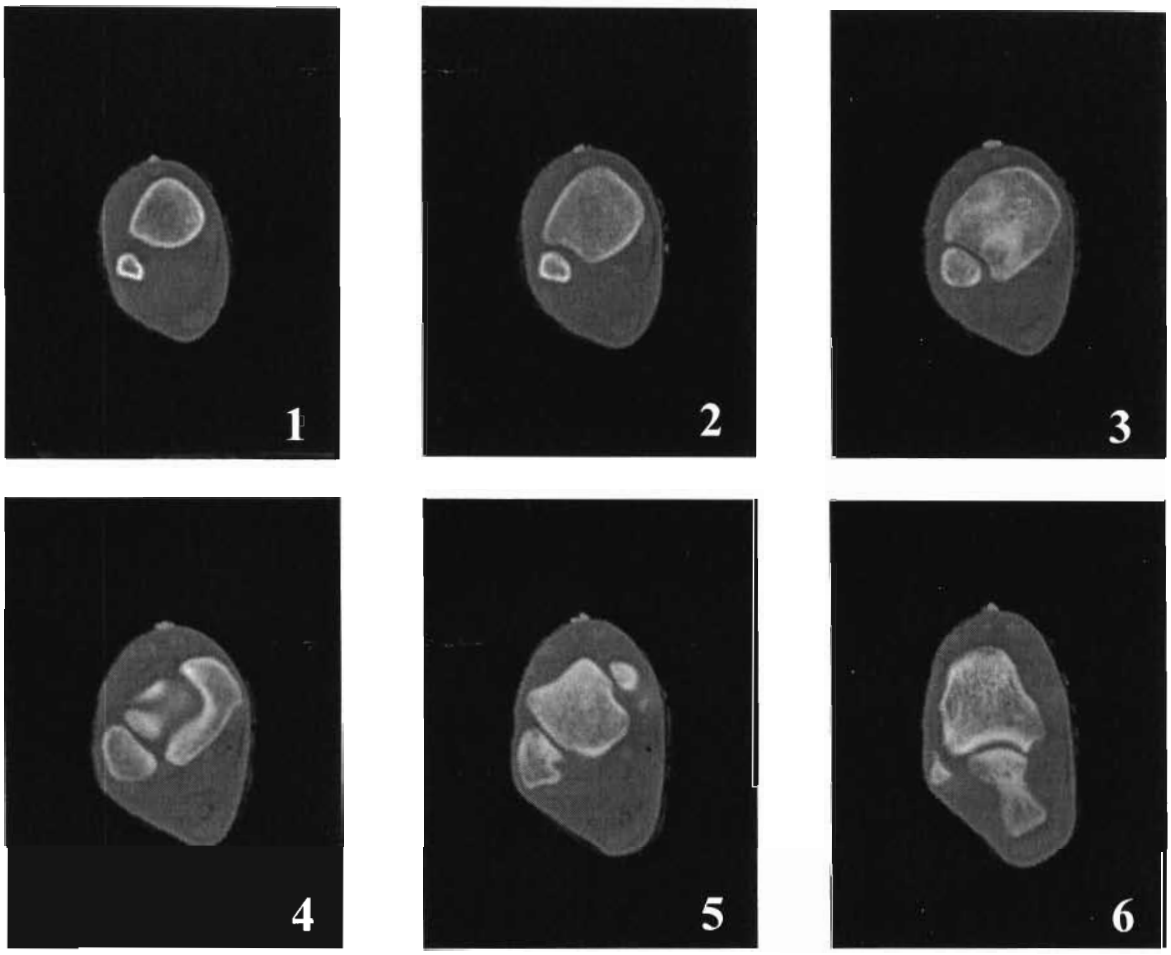

Figure 2.1.1: DICOM Images from the Visual Human Project: These are close-ups of the right ankle with the distal articulation of the tibia and fibula coming into view (top row figs 1-3). Later, the talus and calcaneus appear in the images (bottom row figs 4-6). Scans are shown in 10mm increments. (Note: CT scans look from the inferior up, therefore right of the scan is actually the left and vise versa)

This combination yielded a three-dimensional surface model of the bones as IGES (Initial Graphics Exchange Specification) files for export. The remainder of the proximal tibia and fibula were created with the use of ImageJ 1.32 (Wayne Rasband, National Institutes

of Health, USA) and Microsoft Excel to yield two-dimensional outlines of each individual CT scan for export.

Exported files were then imported into the three-dimensional solid modeling software SolidWorks (TriMech Solutions, LLC, Columbia, MD). SolidWorks along with the COSMOSMotion (TriMech Solutions, LLC, Columbia, MD) package was used to further construct each bone, obtain proper positioning, add necessary components, and run simulations, as described in 2.2 THREE-DIMENSIONAL RECONSTRUCTION. These models were then compared to data obtained from cadaver studies conducted in our laboratory.

2.2 THREE-DIMENSIONAL RECONSTRUCTION:

Three Dimensional Reconstruction using MIMICS:

The male CT scans from the Visual Human Project, spanning the tibia to foot, provided the individual slices from which the three-dimensional anatomy was reconstructed. CT images for the male leg and foot were available in 1.0mm intervals. In order to obtain more detailed features of the foot/ankle complex, the CT images were imported into the software MIMICS where a "mask" for each bone within the foot/ankle complex was created. These "masks" separated the bones from the surrounding soft tissues. To create each "mask", the threshold of the CT scans was varied and then the area representing the bone of interest was covered with a specified color "mask" on the entire stack of CT images.

After each mask was created, a set of "polylines" had to be made and "grown" to create an approximation of each bone's outer perimeter, proximal to distal, for every scan (each 1 mm apart). These "polylines" used fourth order polynomials in their approximations. This set of perimeters was used to create three-dimensional surface models for each bone. For some bones, which possessed multiple perimeters in several consecutive CT scans, two surface files had to be created. Detailed instructions on creating polylines and surface fitting(s) can be found in the MIMICS User Guide. [29] The surface(s) for each bone were then exported as separate IGES surface files and imported into SolidWorks to render as solid objects. In SolidWorks, the ends of each of the surface files were capped. The hollow object was then thickened/filled into a solid body. The bones of the foot/ankle complex were reconstructed in the above fashion for implementation in a variety of biomechanical simulations.

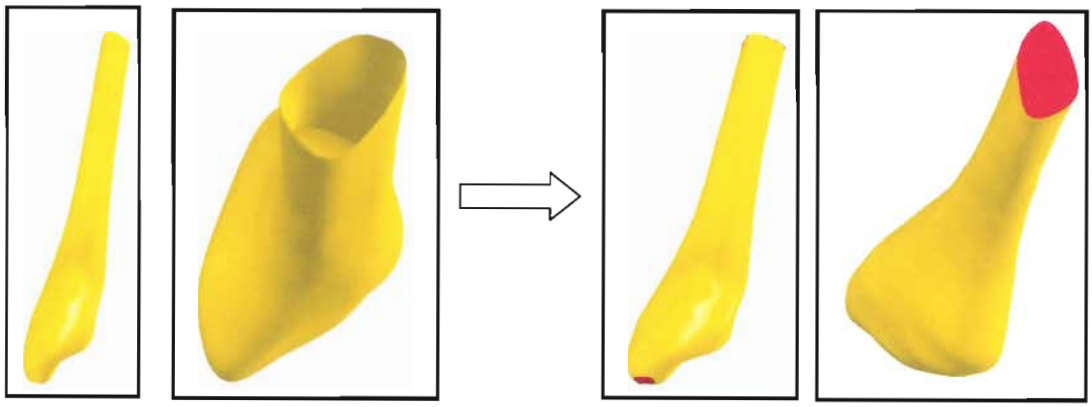

Figure 2.2.1: IGES Surface Files: Left- Surface files imported into SolidWorks. Right- Surface file ends were capped (by creating surfaces on the proximal and distal ends) and the object was filled, thus creating a solid bone. If necessary, the ends could be rounded with a dome feature or capped with a tangent surface, creating an approximation for the rounded ends of each bone.

Three Dimensional Reconstruction using IMAGE J:

To reduce the size of the surface files and subsequent model, the proximal tibia and fibula were reconstructed through ImageJ 1.32, National Institutes of Health, USA, where outlines of each bone on individual CT DICOM scans were created and exported as an XY coordinate map to Microsoft Excel 2000. To accomplish this, first, each CT scan of interest was imported into Image J 1.32. The area of interest was cropped, and using the Thresholding Tool under the "image adjust" and "threshold" tabs, the image, bone, was made a single black color. Another threshold feature was then applied using the threshold tool under the process and binary tabs, this binary threshold is necessary to

run the subsequent steps. The bone (black area) was then filled and outlined using the "Fill Holes" and "Outline" feature under the process and binary tabs. The XY coordinates were then exported using the "Save XY coordinates" option under the analyze tab.

Figure 2.2.2: Bony Outlines: The Image J 1.32 process described above, rendering an outline from the original CT image. This scan is of the right fibula.

Due to the export arrangement of the XY coordinates (all coordinates were arranged from lowest to highest Y values) when imported into Excel, the data had to be separated into two halves. The first half of the coordinates were ordered sequentially from smallest to largest with respect to the X values and the second half were ordered sequentially from largest to smallest with respect to the X values. For example, if there were 40 coordinates, the first twenty would be ordered sequentially from smallest to largest with respect to the X values and the next 20 would be ordered sequentially from largest to smallest with respect to the X values. This function created an outline of the bone in Excel upon graphing. The number of points was then reduced manually to insure no sacrifice was made with respect to shape. This reduction helped to create a smoother surface for each bone, as well as reducing the overall size of the part file. The number of XY coordinates varied for each scan; however, the usual number of coordinates fell

within a range of 15 to 35 points. By manipulating the points manually, the sharp edges on the XY coordinate plot were eliminated before importing into SolidWorks. Moreover, before importing into SolidWorks, one additional XY coordinate had to be included to make the outline a closed loop. To accomplish this, the first point was repeated at the end of the file. Once each outline spanning a particular bone was made, the outlines could be imported into SolidWorks as XYZ coordinates. When all the curves needed were within one SolidWorks "part" file, the curves were lofted together with help of manually added guide curves, thus resulting in a solid object. The number of scans used to recreate the proximal and mid shaft areas of the tibia and fibula varied. Within the proximal region where articulation occurs, scans were used every 5mm; and in the mid shaft region, scans were used every 15-30mm. Both the proximal and mid shaft of the tibia and fibula bones were reconstructed in the above fashion for implementation into a variety of biomechanical simulations.

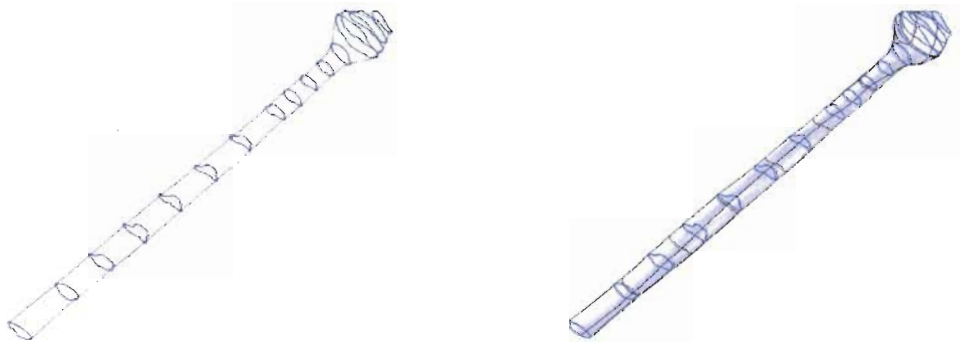

Figure 2.2.3: 3D Reconstruction using Image J, Excel, and SolidWorks:

Left: Proximal fibula outlines (blue) imported into SolidWorks and guide curves (gray)

Right: Lofted outlines together with guide curves to form a solid body

2.3 LOWER EXTREMITY MODELING

Assembly, Alignment, and Overlap Elimination

The separate solid objects within SolidWorks representing each bone were assembled together to form the foot/ankle complex. This was accomplished by bringing each individually made bone ("part file") into an "assembly file" within SolidWorks. After each bone was brought into the "assembly file", they were placed into their initial position by making all three planes of each bone ("part file") coincident. Some of the bones then had to be manually adjusted to make accommodations for the plantar flexion and inversion of the foot, present in the scans of the cadaver from the Visual Human Project. Here, anatomical atlases were consulted to obtain proper neutral positioning.[24, 30, 31] If necessary the bones of the assembly were corrected for interference or overlapping. Overlapping was resolved using the "cavity feature" within SolidWorks; if two bones intersected a cavity was created in the bone with the concave geometry. The cavities were made slightly larger than the intersecting portion of the convex bone (scaled by 0.01%) to create a small space between the two bones. Overlaps were small, and the concavities were kept consistent with the bones. To remedy the sharp edges of each cavity, a fillet was created around the perimeter of each cavity.

2.4 COSMOSMOTION

The three-dimensional SolidWorks model of the lower extremity was then transferred into COSMOSMotion, a software package designed for mechanical system simulation powered by ADAMS® (MSC Software, Santa Ana, CA). COSMOSMotion allowed the application of three-dimensional contacts, springs, forces, and torques. In COSMOSMotion, all solid objects are viewed as rigid non-deformable bodies.

Moving or Grounded Parts:

In COSMOSMotion, each bone included in the simulation must be designated as either a moving or grounded part. Moving Parts were allowed to move during the simulation while the grounded parts were maintained fixed in space.

Rigidly Attached Parts:

This option enables bones to be rigidly attached together and move as a single object. Accordingly, several bones can be fixed together and move as one particular object. For example: the proximal and mid shaft of the fibula were rigidly attached to the distal portion of the fibula, and thus functioned as one part (bone).

Three Dimensional Contacts:

Three-dimensional contacts were established to inhibit intersection of articulating bones during each simulation. These contacts take into account the general interaction of the bones as they collide and rebound while also taking into account the impact and

friction of the collision at all points of contact.[32] Note: When setting up the three-dimensional contacts, each bone must be entered into the contact definition separately, even if the bone is rigidly attached to another. If two bones are rigidly attached (as mentioned above) and have the possibility of intersecting a third bone, each of the three bones (parts) must be entered into the contact definition separately to ensure no intersection takes place. Also to decrease the time needed to run each simulation, an option under the "motion" then "options" then "simulation" tabs called "use precise geometry for 3D contacts" was altered. This variable was changed from 100 to 85.

Addition of Ligaments:

Ligaments were represented as linear springs. Attachment points of each ligament must be at a vertex, circular edge or linear edge of the bone. [32] If these did not exist at the appropriate attachment site(s) for a ligament, one or more split lines were added to the bone in SolidWorks to create a vertex, at the desired site(s). Ligament stiffness values were taken from the literature; these values ranged between 39-129 N/mm.[33-35] All other ligaments not found in the literature were assumed to have a midrange stiffness value of 70-90N/mm. The interosseous membrane was represented by eight springs, each with the stiffness of 400N/mm. This stiffness value was chosen with respect to the length of the tibia and fibula, together with stiffness data found on the interosseous membrane of the forearm.[36] Origin and insertion locations of the ligaments were determined from dissection and anatomical atlases. [24, 30, 31] A pre-

stretch value of 2% was applied to each ligament to represent in situ strain levels, thereby inducing a preload in the ligaments. [37-39]

Addition of Forces and Moments:

All forces or moments created in COSMOS Motion were created as an action only force or moment, meaning that the force or moment is applied on a single rigid body and no reaction forces are calculated.[32] Each force or moment was created as a ramp function meaning the force or moment increased in magnitude with a smooth transition from one value (0N) to the next over a specific time interval. With the application of action only forces and moments, four parameters had to be specified: the component to which force or moment is applied, a grounded reference component to orient the force or moment, the location of where the force or moment is to be applied, and the direction of the force or moment. [32]

Assumptions and Motion Options:

A few assumptions were made in every computational validation study. Friction at each articulation was assumed to be zero. Gravitational forces were considered negligible. Bones were represented as solid objects with a density of 1 g/cm^3.

Exporting Results:

Once each simulation was completed, the results were exported using the motion, export results, and to spreadsheet tabs. Then the desired data was selected and exported to an Excel file.

CHAPTER 3: SYNDESMOTIC INJURY STUDY:

3.1 INTRODUCTION:

Validation of the reconstructed three-dimensional model of the lower leg was determined by comparison to experimental studies. The first comparison focused on a study entitled, "Comparison of the Syndesmotic Staple to the Transsyndesmotic Screw: A Biomechanical Study."[40] This cadaver study was performed to address a controversy existing for the treatment of syndesmotic injuries. The study determined the effects of a external rotation of the foot, and focused on the relative motion between the tibia and fibula, when intact, after a syndesmotic injury, and after repair of the injury. In the cadaver study, two different fixation techniques were analyzed, that of a staple vs. a screw. In our computational model of this cadaver study, only a comparison of the staple fixation was examined, due to the fact the screw relies on the friction of the screw's threads with the bone requiring a friction coefficient along with contact area to be specified for modeling.

Briefly, twenty-one fresh-frozen knee disarticulated specimens were tested on a biaxial servo-hydraulic Instron materials testing machine with an MTS TestStar II controller. All bones distal to the talus were fixed to a platform by screws, leaving only the talus, tibia, and fibula free to move. The first load applied in the cadaver study was a

compressive load of 15lbf that was maintained downward on the tibia throughout all trials. The tibia was then internally rotated, with a submaximal torsional load of magnitude 0-24in-lbf, to simulate external rotation of the foot. Subsequent trials under the same loading conditions were performed; first with the anterior and posterior tibiofibular ligaments, along with 8cm of the distal interosseous membrane closest to the tibiotalar joint, sectioned to simulate a syndesmotic injury. Then the injury was repaired by insertion of a barbed, round, fracture staple in the direction of the anterior tibiofibular ligaments. The variables measured and contrasted to the computational simulation were tibia rotation, fibula rotation relative to the tibia, and fibula translations relative to the tibia in the transverse plane.[40]

3.2 COMPUTATIONAL MODEL of the SYNDESMOTIC INJURY STUDY:

The application of linear and rotational loads to the proximal tibia required the addition of three boundary control structures to the computational model. Two of these structures formed a cylindrical joint, in order to create an axial and torsional axis for the tibia. The movable part of the cylindrical joint was rigidly attached to the proximal shaft of the tibia. The last part added was a platform on which the foot rested. The foot was aligned on the platform so that the calcaneus, first metatarsal, and fifth metatarsal were coincident with the flat surface. The model simulating the syndesmotic injury study was comprised of 14 bones (3 of which were allowed to move), 3 boundary control structures, 26 ligaments (Table 3.2), 1 torsional load, and 1 compressive load. (Fig. 3.2)

The model was first allowed to stabilize for 1 second under the action of ligament preloads. The tibia was then subjected to a 15lbf compressive force over the next second and maintained over the entire length of the simulation. A torsional load of 24in-lbf was then applied over the duration of the third second. Finally, the simulation was allowed to remain under the combined compressive force and torsional load for an additional 0.5 seconds to verify that the simulation had reached equilibrium. To replicate the sectioning of the anterior and posterior tibiofibular ligaments, along with 8cm of the distal interosseous membrane closest to the tibiotalar joint, the springs representing these structures were suppressed. In the final simulation, a barbed fracture staple (22mm in width and 19mm in length) was created and incorporated into the assembly. This simulation mimicked the cadaver study by placing the staple in the direction of the anterior tibiofibular ligament. The staple's two barbs, which were inserted into the tibia and fibula, were modeled as cylindrical joints in COSMOSMotion, allowing only axial rotation.

Two additional calculations had to be performed to obtain some of our desired results. To calculate fibula rotation relative to the tibia, fibula yaws were subtracted from tibia rotations. To calculate anterior/posterior and medial/lateral positions of the fibula relative to the tibia, a beta transformation was performed on the global positions of the fibula with respect to the rotation angle of the tibia. [41]

$\beta = \begin{bmatrix} \cos\alpha & \sin\alpha \\ -\sin\alpha & \cos\alpha \end{bmatrix}$, α is the rotation angle of the tibia

This matrix was multiplied by the global X and Y coordinates of the distal fibula's center of mass to achieve X' and Y' positions in relation to the rotating tibia for each time step during the simulation. The final position was then subtracted from the position before the application of the torque to find the translations.

Ligaments Represented in Models	Stiffness (N/mm)
Anterior Talofibular	90
Anterior Tibiofibular (proximal & distal) (2)	90, 78
Anterior Tibiotalar Calcaneofibular Dorsal Talonavicular (2)	70
Interosseous Membrane (8)	400
Interosseous Talocalcaneal (2) (incorporates the cervical) Lateral Talocancaneal Medial Talocalcaneal Posterior Talocalcaneal Posterior Talofibular	70
Posterior Tibiofibular (proximal and distal) (2)	90, 101
Posterior Tibotalar	80
Tibionavicular	40
Tibiocalcaneal	122

Table 3.2: Stiffness Values- Syndesmotic Injury Study: Stiffness values used for each spring (ligament) present in the models.

(#) Identifies the number of springs used to represent the structure.

Figure 3.2: Syndesmotic Foot Model: Anatomical representation of all the bones of the leg and foot whose three dimensional structure was reconstructed. Springs represent the ligaments and interosseous membrane (all ligaments/springs not pictured for purposes of clarity). 15lbf of compression force and 24in-lb of torsional force were both applied at the cylindrical joint. The tibia, fibula, and talus were free to move while the remaining bones (colored green) were fixed in space.

3.3 RESULTS:

In the experimental syndesmotic study, the tibia demonstrated a rotational increase of 58% when the anterior and posterior tibiofibular ligaments along with 8cm of the interosseous membrane were cut versus intact and decreased after insertion of the staple to a level 15% above intact. The average magnitudes of rotation for intact and cut specimens were 7.47, 11.78 and 8.59 degrees respectively. Fibular external rotation relative to the tibia was found to be 1.77, 3.67, and 1.41 degrees respectively. [40]

In the computational simulations, the tibia demonstrated a slight rotation during the compressive force (0-0.5 degrees), followed by the majority of rotation upon application of torque. Tibial rotation and fibular rotation (relative to the tibia), during the torsional force, increased after simulated injury, and decreased upon staple fixation. Magnitudes of rotation, beginning with the application of the torsional force for the intact, cut and stapled simulations were 4.28, 5.60, and 2.00 degrees respectively. Fibular external rotation relative to the tibia was found to be 1.18, 2.10, and 0 degrees respectively. (Fig. 3.3.1)

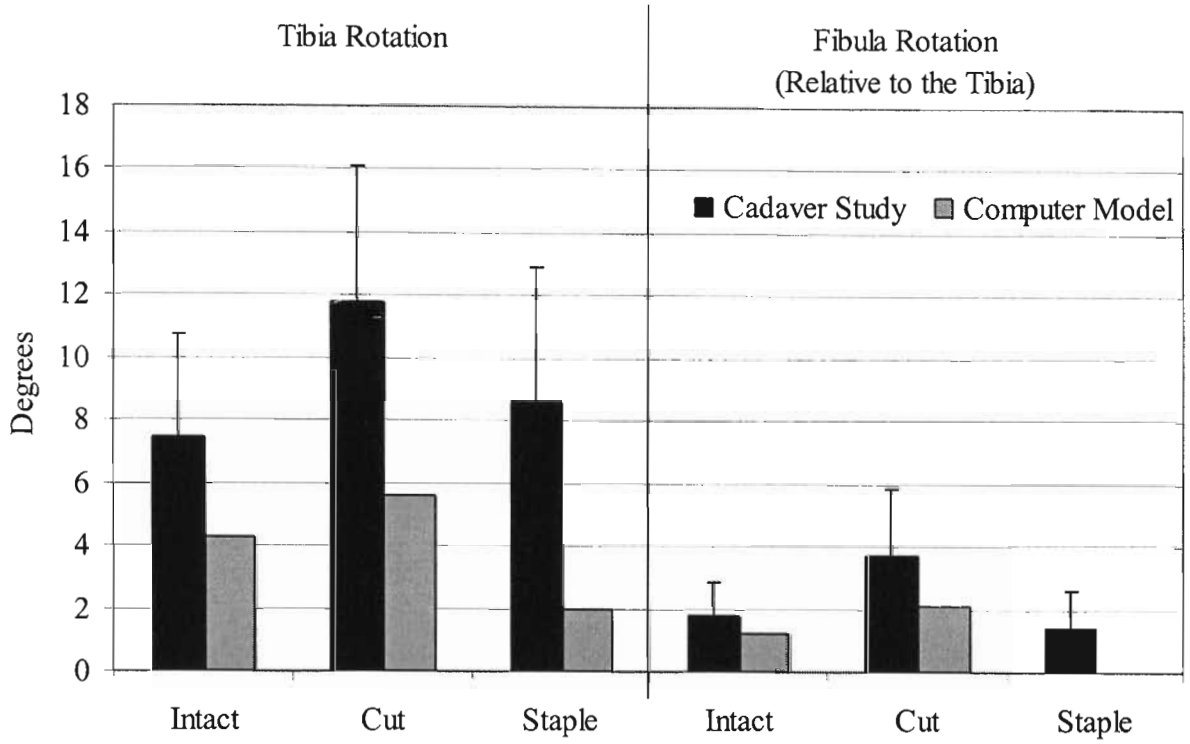

Figure 3.3.1: Rotations of the Tibia and Fibula: Internal rotation of the tibia, relative to the global coordinate system, and external rotation of the fibula, relative to the tibia, during application of 24 in-lb of torque for the configurations evaluated.

Fibular displacement, relative to the tibia, in the anterior/posterior and medial/lateral directions was also experimentally recorded and compared to computational predictions. Computational results for posterior fibular displacement (relative to the tibia), during the torsional force, increased after injury and decreased upon staple fixation (0.73 "posterior", 3.76 "posterior", 0.03 "anterior" mm respectively). Lateral displacement turned into medial displacement, and back to lateral displacement,

with injury and staple fixation (0.60 "lateral", .019 "medial", 0.19 "lateral" mm respectively). (Fig. 3.3.2)

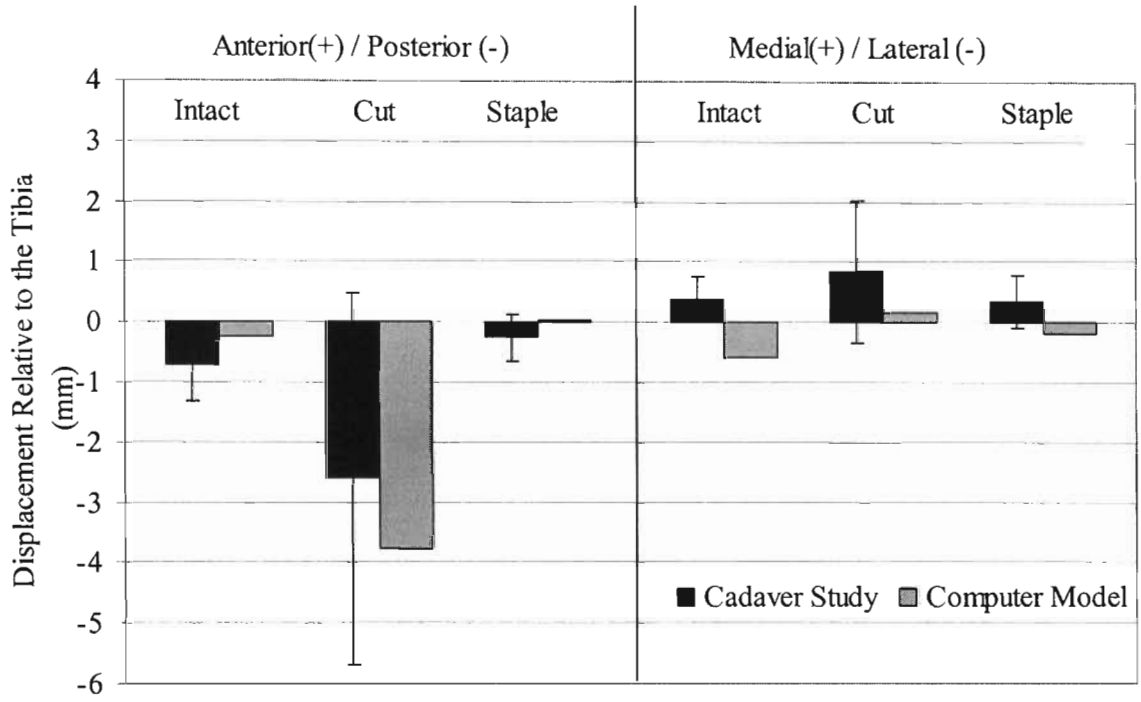

Figure 3.3.2: Fibula Translations: Translations of the fibula, relative to the tibia, in the anterior/posterior and medial/lateral directions, during application of 24 in-lb of torque for the configurations evaluated.

Figure 3.3.3: Bony Movement of the Ankle Complex- Intact Configuration: Foot on the left represents the positioning after application of the preloads, foot in the center represent the positioning after the application of downward force, and foot on the right represents positioning after the application of the torque and equilibrium has occurred. Notice the slight rotation of the tibia (4.28 degrees) after the application of the torque. View is slightly rotated to show all bones.

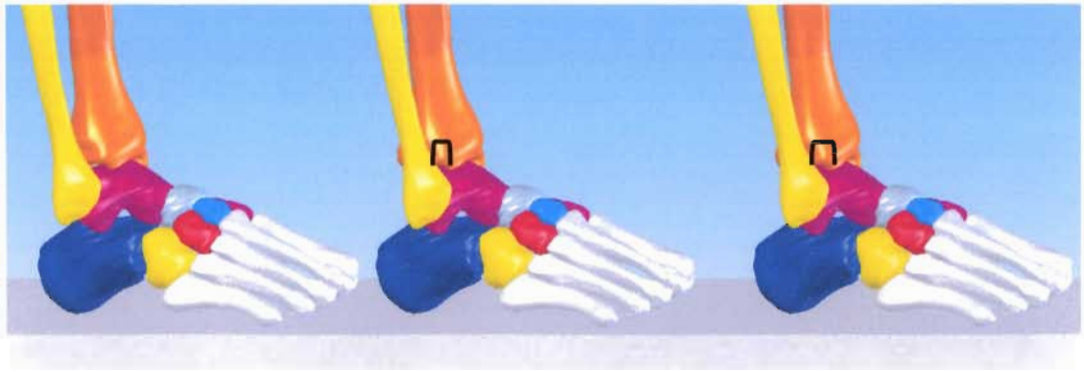

Figure 3.3.4: Bony Movement of the Ankle Complex- Transected Configuration: Foot on the left represents the positioning after application of the preloads, foot in the center represent the positioning after the application of downward force, and foot on the right represents positioning after the application of the torque and equilibrium has occurred. Notice how the space between the tibia and talus is eliminated after the downward force, the slightly greater the rotation of the tibia (5.60 degrees) after the application of the torque, and how the fibula shifts posterior relative to the tibia (3.76mm) after the application of the torque. View is slightly rotated to show all bones.

Figure 3.3.5: Bony Movement of the Ankle Complex- Repaired Configuration: Foot on the left represents the positioning after application of the preloads, foot in the center represent the positioning after the application of downward force, and foot on the right represents positioning after the application of the torque and equilibrium has occurred. Notice how the staple restricts movement after the application of the downward force and torque. View is slightly rotated to show all bones.

This computational model provides the opportunity to predict other functional characteristics that may not be easily obtained in experimental studies, such as the elongation of any ligament, loads experienced in any ligament, and contact forces. Several ligaments displayed the most resistance to the induced rotation with a large resulting force. The calcaneofibular ligament experienced the most loading in two of the three simulations. These ligaments along with the bony architecture are rotational/translational-restricting factors. Forces seen are directly related to the change in length and stiffness of each ligament (spring) (Table 3.3.1). Contact forces were recorded between the talus and tibia, calcaneus and talus, and the talus and fibula. Major

differences can be seen in the contact forces for the talus and fibula between the intact, cut, and staple configurations (Table 3.3.2)

Ligaments	Approximate Force (N) in Major Ligaments Resisting Rotation		
	Intact	Cut	Staple
Anterior Tibiofibular (distal)	64	--	--
Tibionavicular	68	62	45
Calcaneofibular	68	66	62
Tibiocalcaneal	85	70	74

Table 3.3.1: Ligament Forces- Syndesmotic Injury Study: The magnitude of load seen in the major springs (ligaments) resisting movement for the syndesmotic injury study. The forces of the tibionavicular and calcaneofibular ligaments were reduced with the insertion of the staple.

Bony Contacts	Approximate Magnitude of Contact Force (N)		
	Intact	Cut	Staple
Talus and tibia	280	275	275
Calcaneus and talus	240	240	200
Talus and fibula	125	80	240

Table 3.3.2: Contact Forces- Syndesmotic Injury Study: The magnitude contact forces seen in the major articulations of the foot/ankle complex for the syndesmotic injury study. The contact force between the talus and fibula was reduced with transection and increased after staple fixation with respect to the intact configuration.

3.4 MODEL SENSITIVITY:

To assess the sensitivity of the simulations and further validate the computational models, the effect of variations in applied loading magnitude and ligament stiffness values was studied. To illustrate this, the intact syndesmotic model was evaluated while varying certain parameters. Firstly, to insure contact forces are reasonably represented, a simulation was performed with only the application of the 15lbf (67N) compressive load. The contact force that resulted between the tibia and talus accurately reflected the magnitude of this applied force. Then, the torsional load was applied while the magnitude of the compressive force was altered ±50%. This resulted in changes of less than ±4.7% in tibial rotation, ±5.1% in fibular rotation with respect to the tibia, and ±5.6% in fibular translation with respect to the tibia. As seen experimentally, the torsional load was the driving factor for kinematic measurements. Subsequently, the compressive load was held constant at its original value of 15lbf (67N) while the torsional load was changed ±50%. This resulted in changes of expected direction (i.e. increase in load resulted in increases in movement and vice versa), approximately ±48.6% in tibial rotation, ±40.7% in fibular rotation with respect to the tibia, and ±49.2% in either fibular translation with respect to the tibia.

An additional variable that controls the kinematics of the joints are the ligaments, and thus the effect of ligament stiffness variations (±25%) was evaluated for all three configurations. Tables 3.4.1 through 3.4.4 shows the variations due to ligament stiffness. Thus, while model predictions were sensitive to changes in ligament stiffness, a modest

variation that would represent interspecimen variability would not change the conclusions drawn from the models.

Ligament Stiffness	Tibial Rotation (Degrees)		
	Intact	**Cut**	**Staple**
Ligament stiffness decreased by 25%	4.94 (-0.66)	6.51 (+0.91)	2.40 (+0.40)
Original computational model	4.28	5.60	2.00
Ligament stiffness increased by 25%	3.62 (+.66)	5.25 (-0.35)	1.67 (-0.33)

Table 3.4.1: Differences in Tibial Rotations with Changes to Ligament Stiffness

(±#)- Difference from original computational model

Ligament Stiffness	Fibula Rotation with Respect to the Tibia (Degrees)		
	Intact	**Cut**	**Staple**
Ligament stiffness decreased by 25%	1.29 (+0.11)	3.01 (+0.91)	0
Original computational model	1.18	2.10	0
Ligament stiffness increased by 25%	1.13 (-0.05)	1.50 (-0.60)	0

Table 3.4.2: Changes in Fibula Rotation (degrees), with Respect to the Tibia, with Changes to Ligament Stiffness

(±#)- Difference from original computational model

Ligament Stiffness	Anterior (+)/ Posterior (-) Displacement of the Fibula with Respect to the Tibia (mm)		
	Intact	**Cut**	**Staple**
Ligament stiffness decreased by 25%	-0.25 (-0.01)	-3.56 (+0.20)	0.023 (-0.004)
Original computational model	-0.24	-3.76	0.027
Ligament stiffness increased by 25%	-0.19 (+0.05)	-5.86 (-2.10)	0.023 (-0.004)

Table 3.4.3: Changes in Anterior and Posterior Displacements, with Respect to the Tibia, with Changes to Ligament Stiffness

(±#)- Difference from original computational model

Ligament Stiffness	Medial (+)/ Lateral (-) Displacement of the Fibula with Respect to the Tibia (mm)		
	Intact	**Cut**	**Staple**
Ligament stiffness decreased by 25%	-0.70 (-0.10)	0 (-0.17)	-0.26 (-0.07)
Original computational model	-0.60	0.17	-0.19
Ligament stiffness increased by 25%	-0.49 (+0.11)	0.53 (+0.36)	-0.16 (+0.03)

Table 3.4.4: Changes in Anterior and Posterior Displacements, with Respect to the Tibia, with Changes to Ligament Stiffness

(±#)- Difference from original computational model

3.5 DISCUSSION:

The present computational models of external rotation of the foot revealed a capability to predict differences in joint kinematics with varying conditions of the syndesmosis and ligament deficiencies. In the syndesmotic study, all three models predicted tibial rotations, showing a trend similar to that of the cadaver study. Fibula rotation relative to the tibia showed accuracy in both the results and trend seen when compared to the cadaver study. (Fig. 3.3.1) The correct trend for fibula translation, relative to the tibia, was predicted in the anterior/posterior direction. Absolute values for translations in the medial/lateral direction proved harder to predict, but showed the correct trend for changes among the configurations. (Fig. 3.3.2)

Differences that should be noted between the computer simulation and cadaver study are: simulation modeled a particular foot whereas the cadaver study included 21 feet; ligaments were represented as a linear springs with an in situ strain displacing each ligament beyond its toe region; bony architecture was partially dependent upon surface fitting techniques within computer programs; and ligament stiffness and placement were controlled by the simulator. The main reason the staple simulation differed from the experimental study was that the staple acted as a rigid body that could not deform nor displace; only rotational movement was allowed on the two posts of the staple.

CHAPTER 4: ANKLE INVERSION STABILITY STUDY

4.1 INTRODUCTION

Validation of the reconstructed three-dimensional model of the lower leg continued by further comparison to experimental studies. The second comparison focused on a study entitled, "Elongation Behavior of Calcaneofibular and Cervical Ligaments during Loads Applied in an Open Kinetic Chain," which determined the elongation behavior of the calcaneofibular and cervical ligaments while also measuring the calcaneal inversion angle under an applied inversion load.[42] Results of the cadaver study indicated a significant increase in elongation of the cervical ligament in the absence of the calcaneofibular ligament during loading.

Briefly, nine fresh-frozen knee disarticulated specimens with their distal forefoot removed were tested using a manual and mechanical method of inversion. The mechanical method of inversion will be the focus of our computational comparison. The tibia was held fixed using an intramedullary rod and fixation jig. All other bones were free to move. The load was applied using a bicortical, 5mm machine screw placed lateral to medial into the calcaneus, 2cm up from the heel pad, and midway between the distal insertion points of the calcaneofibular and cervical ligaments. A cable was attached from the lateral insertion of the screw, under the plantar surface, to a pulley system and then to

a 10 lb weight, thus inducing the inversion moment. Experimental trials were run under conditions in which all ligaments were intact and where the calcaneofibular ligament was transected. Elongation of calcaneofibular ligament (during the intact trial) and cervical ligaments lengths were recorded as well as the calcaneal inversion angles. [42]

Clinically the inversion test helps to detect a torn anterior talofibular ligament and torn calcaneofibular ligament. This test is performed by having the patient sit on the examining table with their legs hanging off the side. The examiner uses one or both hands to cup the calcaneus and talus and an inversion moment applied. If a gapping movement occurs between the talus and tibia/fibula, then the anterior talofibular and calcaneofibular ligaments are torn.

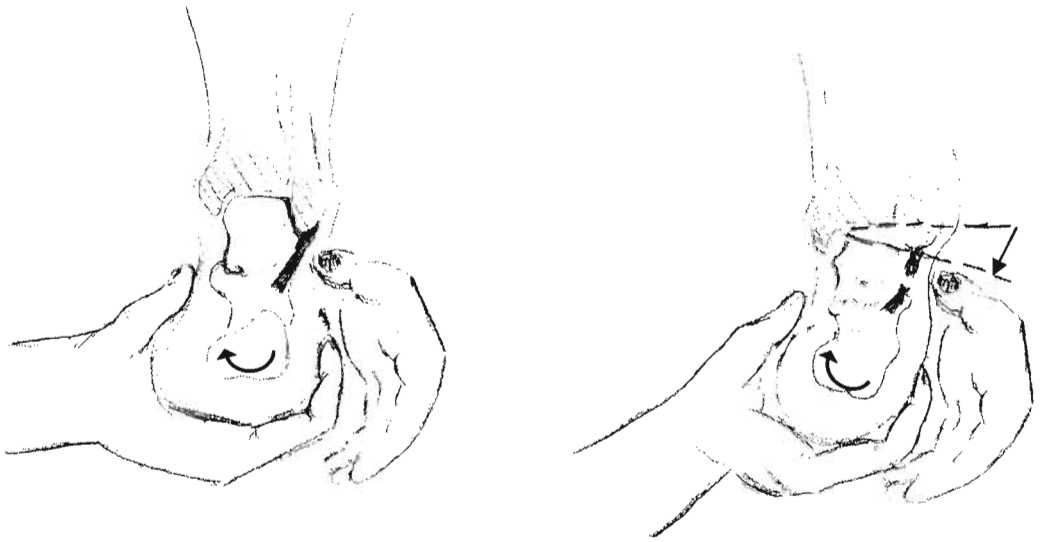

Figure 4.1: Talar Tilt Test: This test in which the calcaneus is inverted helps to evaluate the stability of the anterior talofibular and calcaneofibular ligaments. If these ligaments are torn gapping will occur between the tibia and talus (right). (picture redrawn and modified from [28])

4.2 COMPUTATIONAL MODEL of the ANKLE INVERSION STABILITY STUDY:

The computational model for the ankle inversion stability study was comprised of 9 bones (8 of which were allowed to move), 39 ligaments (Table 4.2), 1 force guiding structure, and 1 linear force. (Fig. 4.2) One grounded structure (other than the bones) was needed for orientation of the inversion force.

The computational model was first allowed to stabilize for 2 seconds under the action of ligament preloads. The tibia was maintained static over the entire length of the simulation. The inversion load of 10 lb was then applied to the plantar surface of the

calcaneus midway between the distal insertion points of the calcaneofibular and cervical ligaments. The load was applied over the third second and maintained for the remainder of the simulation until equilibrium was reached. In the subsequent trials, the sectioning of the calcaneofibular ligament was replicated by suppressing the appropriate spring.

To obtain the inversion angle of the calcaneus, the measuring tool was used in SolidWorks to display the distance between the two selected points on the calcaneus in relation to the X, Y, and Z-axes before and after the simulations. The inverse tangent of, delta Y/delta Z, was then performed to calculate the inversion angle.

Ligaments Represented in Models	Stiffness (N/mm)
Anterior Talofibular	90
Anterior Tibiofibular (proximal & distal) (2)	90, 78
Anterior Tibiotalar Bifurcate (Calcaneocuboid, Calcaneonavicular) (2) Calcaneofibular Dorsal Calcaneocuboid (2) Dorsal Cuboideonavicular Dorsal Cuneocuboid (2) Dorsal Talonavicular (2)	70
Interosseous Membrane (8)	400
Interosseous Talocalcaneal (2) (incorporates the cervical) Lateral Talocancaneal Long Plantar Medial Talocalcaneal Plantar Calcaneonavicular (spring) (2) Plantar Cuboideonavicular Plantar Cuneocuboid Posterior Talocalcaneal Posterior Talofibular	70
Posterior Tibiofibular (proximal and distal) (2)	90, 101
Posterior Tibotalar	80
Short Plantar	70
Tibionavicular	40
Tibiocalcaneal	122

Table 4.2: Stiffness Values- Ankle Inversion Stability Study: Stiffness values used for each spring (ligament) present in the models

(#) Identifies the number of springs used to represent the structure.

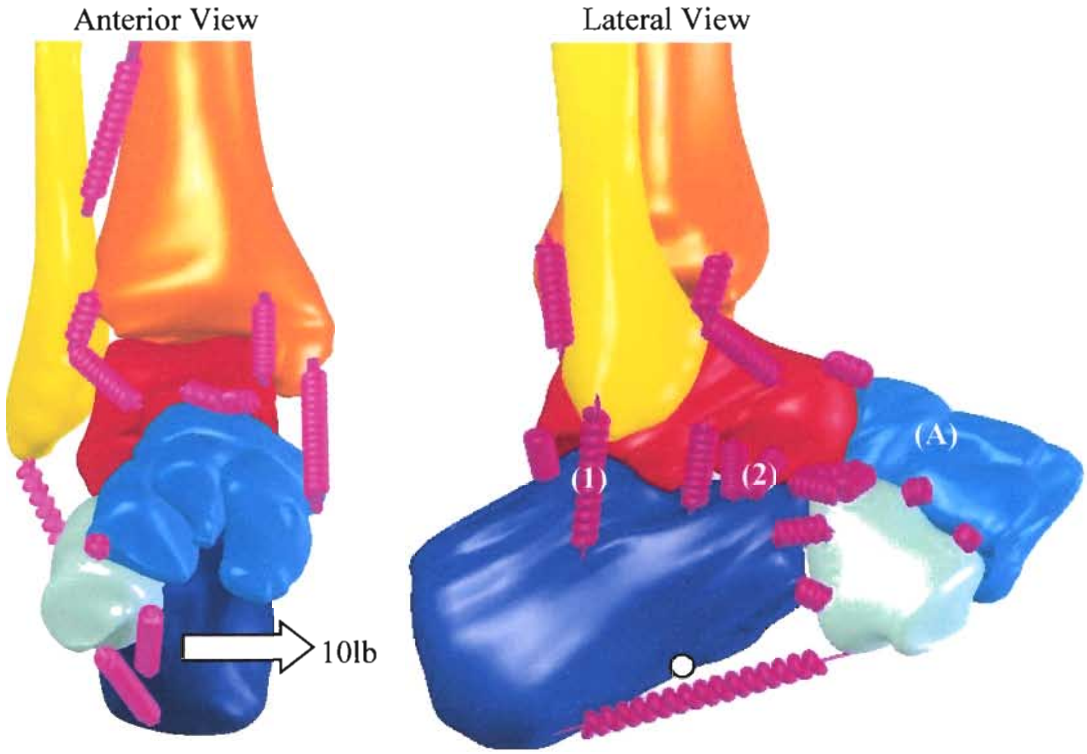

Figure 4.2: Ankle Inversion Stability Foot Model: Anatomical representation of all the bones of the leg and foot whose three dimensional structure was reconstructed. Proximal portions of the tibia and fibula are not pictured, but present in the model. The tibia was fixed, and all other bones were allowed to move. The navicular and three cuneiform bones were fixed together and moved as one object (A). The application of the 10lb force (arrow and circle) in the model was applied to the plantar surface and midway between the distal attachment points of the calcaneofibular (1) and cervical (2) ligaments. All ligaments/springs not pictured for purposes of clarity.

4.3 RESULTS:

As shown in the ankle stability study, the calcaneofibular elongation was measured to be 0.5±0.25 mm under the action of the 10lb inversion moment. The starting position of all specimens was calcaneal varus at an average of 7.9±6 degrees. The inversion angle after application of the moment was measured at 18.3 and 25.8 degrees for intact and transected calcaneofibular ligament, respectively. The elongation ratio for the cervical ligament was calculated to be 1.86±0.37 when comparing cut relative to intact. [42]

In the corresponding computational simulations, the calcaneofibular elongation was found to be 0.55 mm. The starting position was found to be calcaneal varus at 3.1 degrees. The inversion angle after the application of the moment was measured at 9.4 and 17.4 degrees for intact and transected calcaneofibular ligament states, respectively. A comparison of the computational model to the cadaver study demonstrated a striking similarity in behavior patterns for both calcaneofibular elongation and inversion angles. (Figs. 4.3.1 & 4.3.2) No elongation ratio for the cervical ligaments could accurately be calculated, due to the fact that there was no notable extension in this ligament.

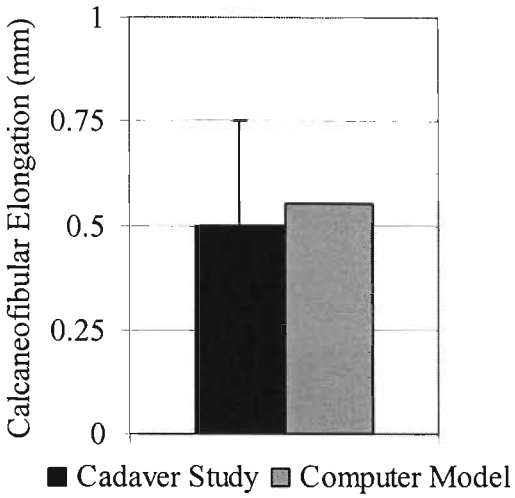

Figure 4.3.1: Calcaneofibular Elongations: Elongation of the calcaneofibular ligament in the intact state of the cadaver study and the computational model.

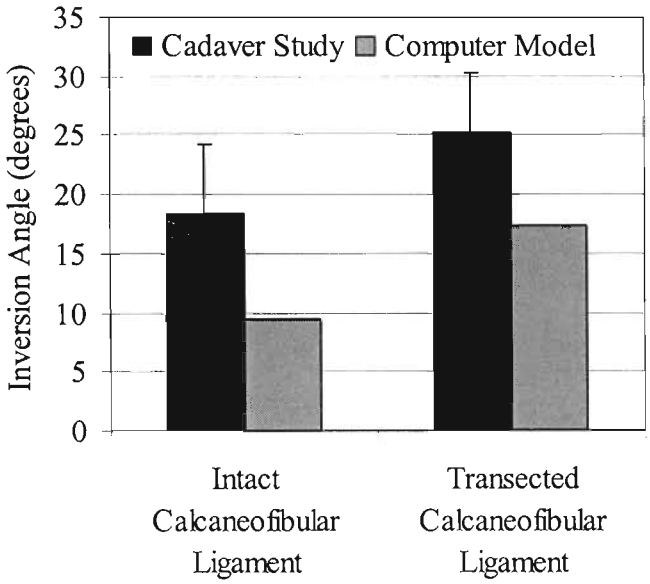

Figure 4.3.2: Inversion angles: Inversion angles of the calcaneus before (intact) and after transection of the calcaneofibular ligament in the cadaver study and computational model.

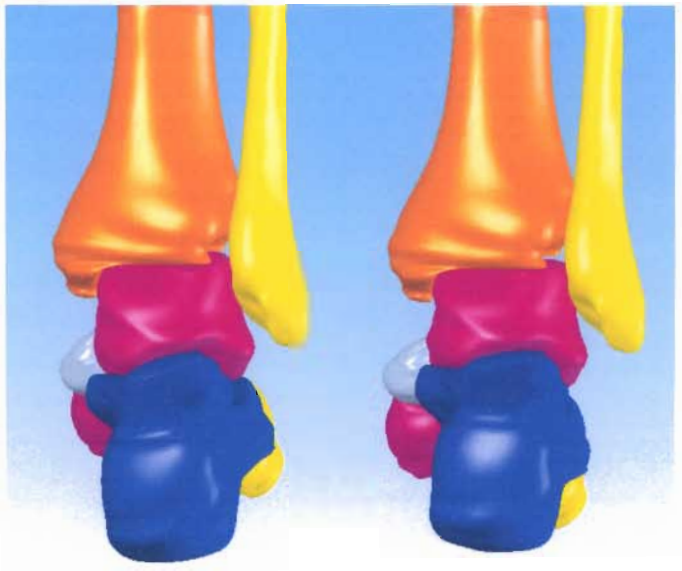

Figure 4.3.3: Bony Movement of the Ankle Complex- Intact Configuration: Foot on the left represents the positioning before the start of the simulation and foot on the right represents positioning after the application of the inversion force. Notice how the movement occurs correctly between the talus and calcaneus.

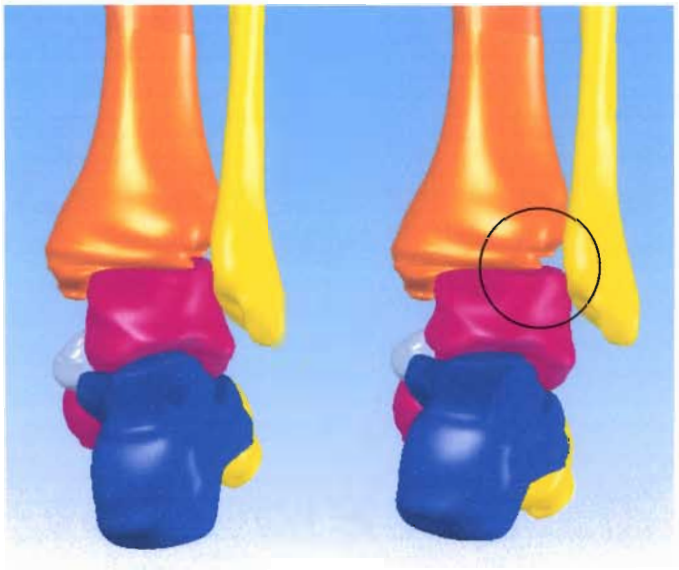

Figure 4.3.4: Bony Movement of the Ankle Complex- Transected Configuration: Foot on the left represents the positioning before the start of the simulation and foot on the right represents positioning after the application of the torque and equilibrium has occurred. Notice the excessive movement of the talus and the gapping in between the tibia and talus (circled). This gapping is an indication of a torn calcaneofibular ligament.

Additional information may be garnered from this computational model that cannot be readily measured experimentally. Several ligaments displayed the most resistance to inversion with a large resulting force. The calcaneofibular ligament experienced the greatest load in the intact simulation and the lateral talocalcaneal ligament increased in load magnitude when the calcaneofibular ligament was transected. These ligaments along with the bony architecture are the inversion restricting factors. Forces seen are directly related to the change in length and stiffness of each ligament

(spring). (Table 4.3.1) Contact forces were recorded between the talus and tibia, calcaneus and talus, and the talus and fibula. Major differences can be seen in the contact forces for the talus and tibia between the intact and transected configurations (Table 4.3.2)

Ligaments	**Approximate Force (N) in Major Ligaments Elongating and Resisting Inversion**	
	Intact	**Cut**
Calcaneofibular	88	--
Lateral Talocalcaneal	42	100
Posterior Tibiofibular (distal)	76	105
Anterior Fibulotalar	58	50
Dorsal Calcaneocuboid (lateral)	30	60

Table 4.3.1: Ligament Forces- Ankle Inversion Stability Study: The magnitude of load seen in the major springs (ligaments) resisting movement during the inversion study. When the calcaneofibular ligament was suppressed, as expected the major increase in force was seen in several of the ligaments on the lateral aspect of the foot and ankle.

Bony Contacts	Approximate Magnitude of Contact Force (N)	
	Intact	Cut
Talus and tibia	270	175
Calcaneus and talus	175	160
Talus and fibula	170	175

Table 4.3.2: Contact Forces- Ankle Inversion Stability Study: The magnitude contact forces seen in the major articulations of the foot/ankle complex for the ankle inversion stability study. The contact force between the talus and tibia greatly reduces with transaction of the calcaneofibular ligament.

4.4 MODEL SENSITIVITY:

The sensitivity of these models to loading conditions were discussed in section 3.4 MODEL SENSITIVITY, therefore this section will just discuss the changes seen in the models due to changes in ligament stiffness. The effect of ligament stiffness variations (±25%) was evaluated for both intact and cut configurations. Tables 4.4.1 and 4.4.2 shows the variations due to ligament stiffness. Thus, while model predictions were sensitive to changes in ligament stiffness, a modest variation that would represent interspecimen variability would not change the conclusions drawn from the models.

Ligament Stiffness	Calcaneal Inversion Angle (degrees)	
	Intact	**Cut CFL**
Ligament stiffness decreased by 25%	9.92 (+0.51)	18.44 (+1.07)
Original computational model	9.41	17.37
Ligament stiffness increased by 25%	9.18 (-0.23)	16.49 (-0.88)

Table 4.4.1: Changes in the Calcaneal Inversion with Changes to Ligament Stiffness

(±#)- Difference from original computational model

Ligament Stiffness	Elongation of the Calcaneofibular Ligament (mm)
	Intact
Ligament stiffness decreased by 25%	0.71 (+0.16)
Original computational model	0.55
Ligament stiffness increased by 25%	0.46 (-0.09)

Table 4.4.2: Changes in Elongation of the Calcaneofibular Ligament with Changes to Ligament Stiffness

(±#)- Difference from original computational model

4.5 DISCUSSION:

As indicated by the results from the inversion study, calcaneofibular elongation was predicted accurately. The increase in inversion angles for the calcaneus from intact to cut in the cadaver study was calculated to be 7.5 degrees, while the computational model predicted an increase of 8 degrees for the comparable trials. These inversion angle values fall within the range of magnitudes given in the study conducted by Kjaersgaard-Andersen et al. [43] Even though an elongation ratio for the cervical ligament could not be calculated (due to lack of length change in this ligament), the computational model did show a ratio of 2.17 for the lateral talocalcaneal ligament compared to the ratio of 1.86 in the cadaver study calculated for the cervical ligament.[42] Due to their close proximity, it is possible that the lateral talocalcaneal ligament in our computational model is restricting the elongation of the cervical ligament. If the stiffness of the lateral talocalcaneal ligament is reduced, elongation does occur in the cervical ligament.

Differences that should be noted between the computer simulation and cadaver study are: simulation modeled a particular foot whereas the cadaver study included 9 feet; ligaments were represented as a linear springs with an in situ strain displacing each ligament beyond its toe region; bony architecture was partially dependent upon surface fitting techniques within computer programs; slight differences in load application and ligament stiffness and placement were controlled by the simulator. Also all bones were viewed as rigid body that could not deform.

CHAPTER 5: MECHANICAL LAXITY STUDY

5.1 INTRODUCTION

Ankle instability is a common problem after injury to ligaments. The preceding two chapters focused on previous cadaver studies conducted in our laboratory; this chapter will try to reduce any bias by simulating a cadaver study from an outside laboratory. The study chosen was entitled "Assessment of the Ankle-Subtalar-Joint-Complex Laxity Using an Instrumented Ankle Arthrometer: An Experimental Cadaveric Investigation."[44] This study focused on total anterior/posterior displacement and inversion/eversion rotations under applied loading conditions on intact, anterior talofibular transected, and anterior talofibular and calcaneofibular transected ankle joints. Other studies have also been conducted on ankle laxity; however, the major advantage of this study is that the investigators compared the measured movements achieved from an ankle arthrometer to the actually bony movements as measured by an instrumented spatial linkage physically attached to the bones.[44-48] The bony movements will be contrasted to the similarly designed computer simulations.

Briefly, six fresh, frozen cadaver lower legs without evidence of injury to any ligaments that would affect anterior/posterior movement as well as inversion/eversion

movement within the ankle complex were used by Kovalesky et al [44]. The Lower legs were harvested approximately 25cm above the ankle joint. A rod was screwed into the medullary cavity of the tibia for mounting purposes; the end of this rod was clamped to a table. The ankle arthrometer was attached with all feet in the neutral position. [44] The neutral position can be defined as when the foot is neither pronated or supinated, and the sagittal plane bisector of the calcaneus is at 90 degrees to the supporting surface.[49]

The arthrometer consisted of the following items: an adjustable plate that was fixed to the foot via a dorsal clamp, a posterior heel pad, and medial and lateral heel clamps. This foot plate was attached to a load cell with a loading handle to induce the linear and torsional loads. A tibial pad and restraining straps held the lower leg in place for the tests. The arthrometer had a six degree of freedom spatial kinematic linkage connecting the tibial pad and the foot plate.[44, 45] In this particular study, bony motion was measured using a second 6 degree of freedom spatial linkages attached directly to the tibia and calcaneus. This linkage measured calcaneal motion relative to the tibia, for both anterior/posterior and inversion/eversion. Total anterior/posterior displacement is equal to the sum of anterior translation and posterior translation. Total inversion/eversion rotation is equal to the sum of inversion rotation and eversion rotation. Anterior and posterior displacements were measured under a load of 125N, while inversion and eversion rotations used a torque of 4000N-mm. [44]

Basically this arthrometer can be used to place quantitative assessments on standard tests performed by physicians. Two standard tests performed are the Talar Tilt Test, shown in Figure 4.4, and Anterior Drawer Test, shown in Figure 5.1. These tests

are administered to determine if a deficiency exists in a lateral ankle ligament (ATFL or CFL). The Anterior Drawer test helps to detect a torn anterior talofibular ligament. This test is performed by having the patient sit on the examining table with their legs hanging off the side. The examiner then grasps the distal aspect of the leg around the tibia and fibula with one hand, and cups the calcaneus with the other. An anterior force is then applied to the calcaneus while pushing back on the tibia. There should be no forward movement of the talus with respect to the tibia.

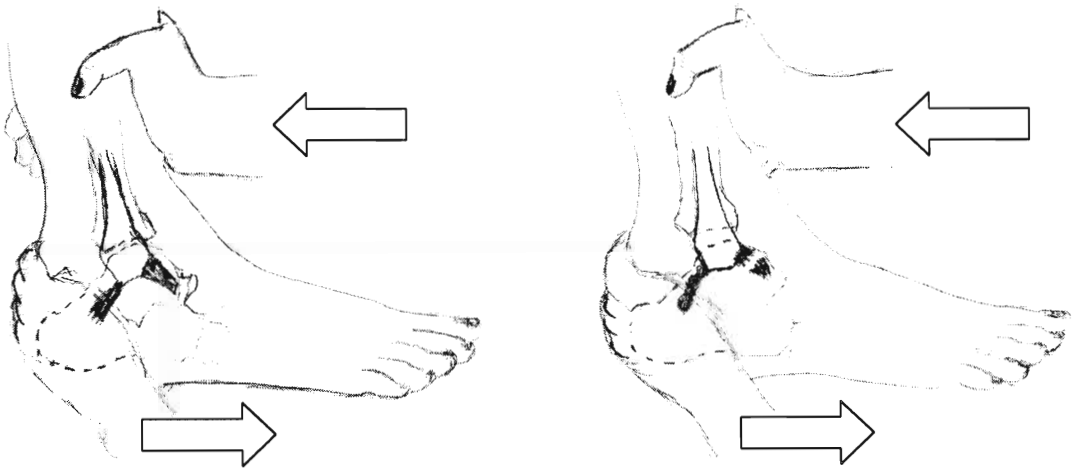

Figure 5.1: The Anterior Draw Sign Test: This test evaluates the anterior talofibular ligament. If this ligament is torn, an anterior translation of the foot will occur (right). (picture redrawn and modified from [28])

5.2 COMPUTATIONAL MODEL of the LAXITY STUDY

Separate simulations must be performed for each anterior/posterior and inversion/eversion force application. In both computational simulations (anterior/posterior and inversion eversion), the tibia was held fixed. The talus and fibula were free to move, and the remaining bones were rigidly attached to the foot platform.

In the anterior/posterior configurations, the footplate was maintained parallel with the XY plane, and no rotation was allowed. A load of 125N was applied normal to a face of the foot in either the anterior or posterior direction. The transected configurations included first the suppression of the spring representing the anterior talofibular ligament, followed by the suppression of the spring representing the calcaneofibular ligament. The model of the anterior/posterior laxity was comprised of 6 bones (with talus and fibula being unconstrained, the tibia fixed, and the calcaneus, navicular, cuboid, and foot platform being regarded as one rigid body), 26 ligaments (Table 5.2), and 1 linear force (Fig. 5.2.1). It was assumed that no movement of the midfoot/forefoot occurred due to the presence of the dorsal clamp in the cadaver study.

Figure 5.2.1: Anterior/Posterior Laxity Foot Model: Anatomical representation of all the bones of the leg and foot whose three dimensional structures was reconstructed. Proximal portions of the tibia and fibula are not pictured, but present in the model. 125N of force was applied normal to the foot platform in two different simulations (anterior and posterior). The tibia was fixed (orange), talus and fibula were free to move (red and yellow respectively); the calcaneus, navicular, cuboid, and foot platform were rigidly attached to each other and moved as one solid body (green).

In the inversion/eversion configurations, a torque of 4000N-mm was applied to the foot platform around a designated axis replicating that of the axis in the cadaver study. The transected configurations included first the suppression of the spring representing the anterior talofibular ligament, followed by the suppression of the spring representing the calcaneofibular ligament. The model of the inversion/eversion laxity was comprised of 6 bones (with talus and fibula being totally unconstrained, the tibia

fixed, and the calcaneus, navicular, cuboid, and foot platform being regarded as one rigid body), 26 ligaments (Table 5.2), and 1 linear force (Fig. 5.2.2). An assumption was made that no movement of the forefoot occurred do to the presence of the dorsal clamp in the cadaver study.

Figure 5.2.2: Inversion/Eversion Laxity Foot Model: Anatomical representation of all the bones of the leg and foot whose three dimensional structures were reconstructed. A torque of 4000N-mm was applied to the foot platform in two different simulations (inversion and eversion). The tibia was fixed (orange), talus and fibula were free to move (red, and yellow respectively); the calcaneus, navicular, cuboid, and foot platform were rigidly attached to each other and moved as one solid body (green). Rotation occurred around a fixed axis, mimicking the axis in the cadaver study.

Ligaments Represented in Models	Stiffness (N/mm)
Anterior Talofibular	90
Anterior Tibiofibular (proximal & distal) (2)	90, 78
Anterior Tibiotalar Calcaneofibular Dorsal Talonavicular (2)	70
Interosseous Membrane (8)	400
Interosseous Talocalcaneal (2) Lateral Talocancaneal Medial Talocalcaneal Posterior Talocalcaneal Posterior Talofibular	70
Posterior Tibiofibular (proximal and distal) (2)	90, 101
Posterior Tibotalar	80
Tibionavicular	40
Tibiocalcaneal	122

Table 5.2: Stiffness Values- Laxity Studies: Stiffness values used for each spring (ligament) present in the models.

(#) Identifies the number of springs used to represent the structure.

Each computational model was first allowed to stabilize for 1.5 second under the action of ligament preloads. Then, a force of 125N, in the anterior/posterior direction, or a torque of 4000N-mm, in the inversion/eversion direction, was then applied to the foot platform over the next 2 seconds, and maintained over the remainder of the simulation until equilibrium was reached. In the subsequent trials, the sectioning of the anterior talofibular and calcaneofibular ligaments were replicated by suppressing the appropriate springs.

5.3 RESULTS

As shown in the Ankle Laxity Study conducted by Kovaleski et al., total anteroposterior bony displacement measured with the spatial linkage attached to the tibia/calcaneus was measured to be 7.43±3.1, 11.38±3.8, 12.77±4.8mm for Intact, ATFL transected, and ATFL+CFL transected respectively. Total inversion-eversion bony rotation was measured to be 16.66±2.4, 19.14±3.4, 25.37±4.8 degrees for Intact, ATFL transected, and ATFL+CFL transected respectively.

In the corresponding computational simulations, total anteroposterior displacement was measured to be 6.8, 7.6, 8.5mm for Intact, ATFL transected, and ATFL+CFL transected respectively. A comparison of the computational model's and the cadaver study's results demonstrated similarity in behavior patterns after each transection. (Figure 5.3.1) In the computational model, after transaction of the ATFL, additional laxity occurred in both the anterior and posterior directions and after the transection of the CFL, additional laxity occurred in the posterior direction. Total inversion/eversion rotation was measured to be 9.7, 9.7, 20.4degrees for Intact, ATFL transected, and ATFL+CFL transected respectively. A comparison of the computational model to the cadaver study demonstrated similarity in behavior pattern after the transection of the CFL. (Figure 5.3.2) In the computational model, the transection of the ATFL had little/no effect on inversion/eversion rotation of the ankle, however after the transection of the CFL a major difference was observed in the inversion rotation.

Computational Configurations	Anterior/Posterior Displacements (mm)	Inversion/Eversion Rotations (degrees)
Intact Ankle	3.5/3.3	6.9/2.8
Transected ATFL	3.8/3.8	6.8/2.9
Transected ATFL+CFL	3.8/4.7	18.0/2.4

Table 5.3.1: Total Anteroposterior Displacement and Inversion/Eversion Rotation in the Computational Simulations

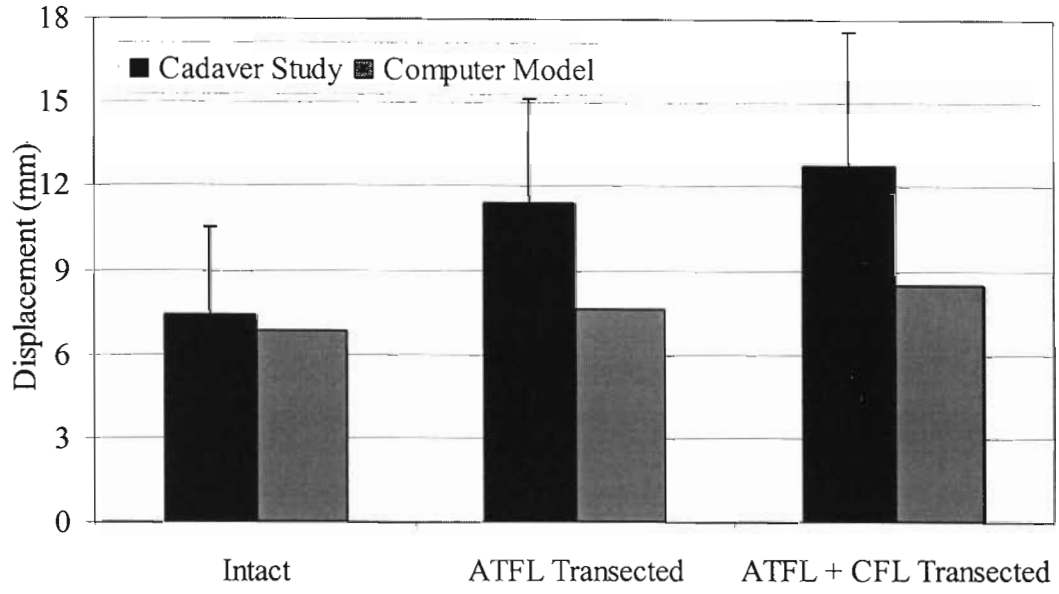

Figure 5.3.1: Anteroposterior Displacement for the Laxity Study: The simulations were able to predict anterior/posterior laxity within the standard deviations of the cadaver study. The simulation changes after transections were smaller than that of the cadaver study, however, an increasing trend is exhibited after each transection.

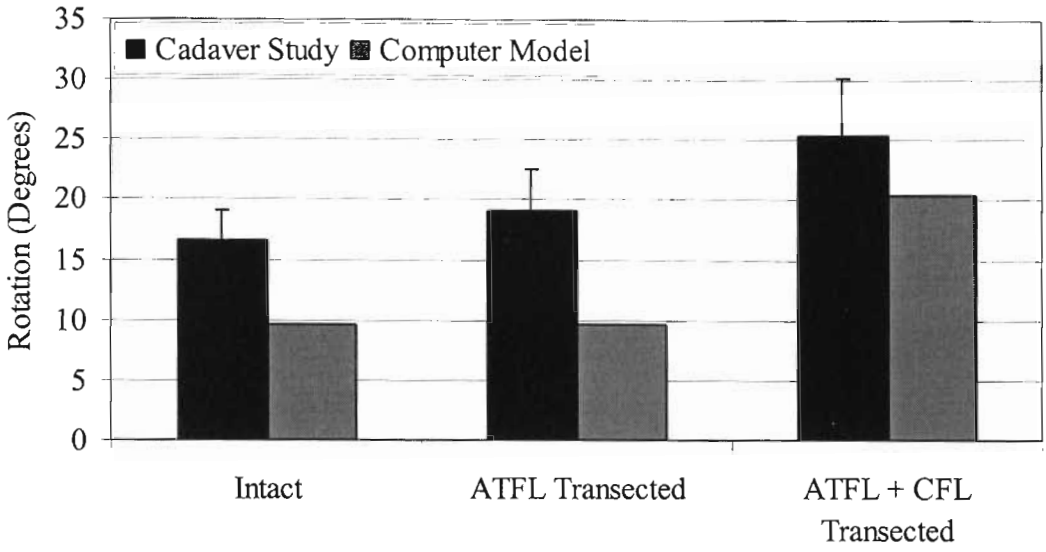

Figure 5.3.2: Rotation for the Laxity Study: The computational models demonstrated no change in inversion/eversion laxity due to the transection of the ATFL; however, after the transection of the CFL, more than double the rotation occurred.

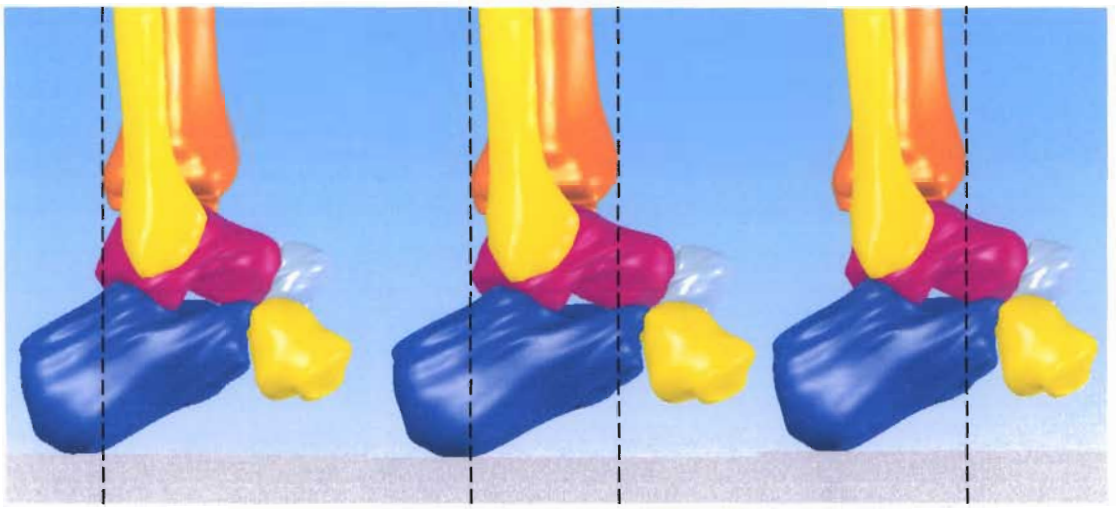

Figure 5.3.4: Bony Movement of the Ankle Complex- Intact Configuration: Foot on the left represents the positioning after application of the posterior force, foot in the center represents the starting position, and foot on the right represents positioning after the application of the anterior force. Notice the slight anterior and posterior movement of the talus and calcaneus with respect to the tibia.

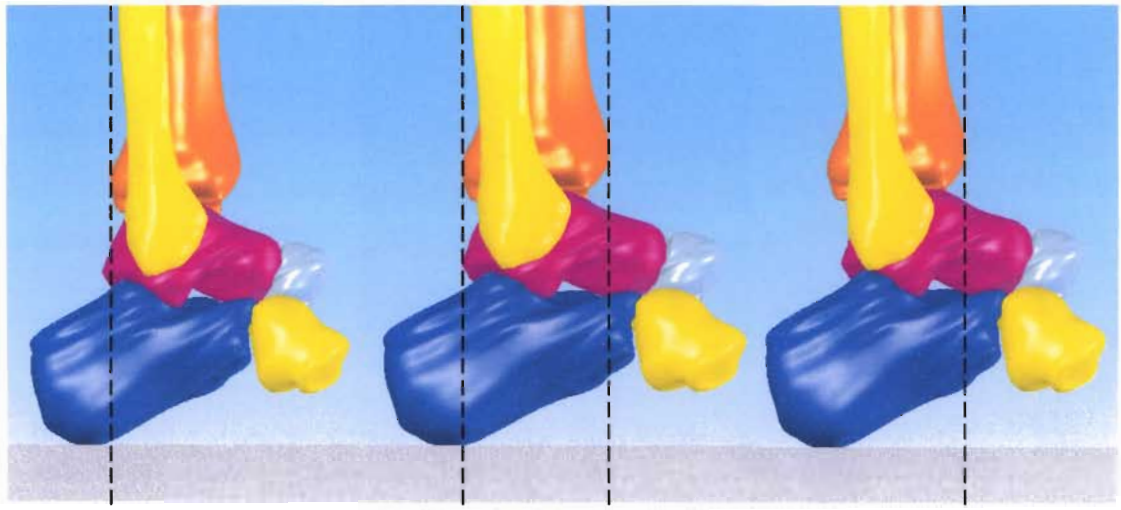

Figure 5.3.5: Bony Movement of the Ankle Complex- ATFL Suppressed Configuration: Foot on the left represents the positioning after application of the posterior force, foot in the center represent the starting position, and foot on the right represents positioning after the application of the anterior force. The slight increase in both anterior and posterior movement of the talus and calcaneus with respect to the tibia is difficult to distinguish from Figure 5.3.4.

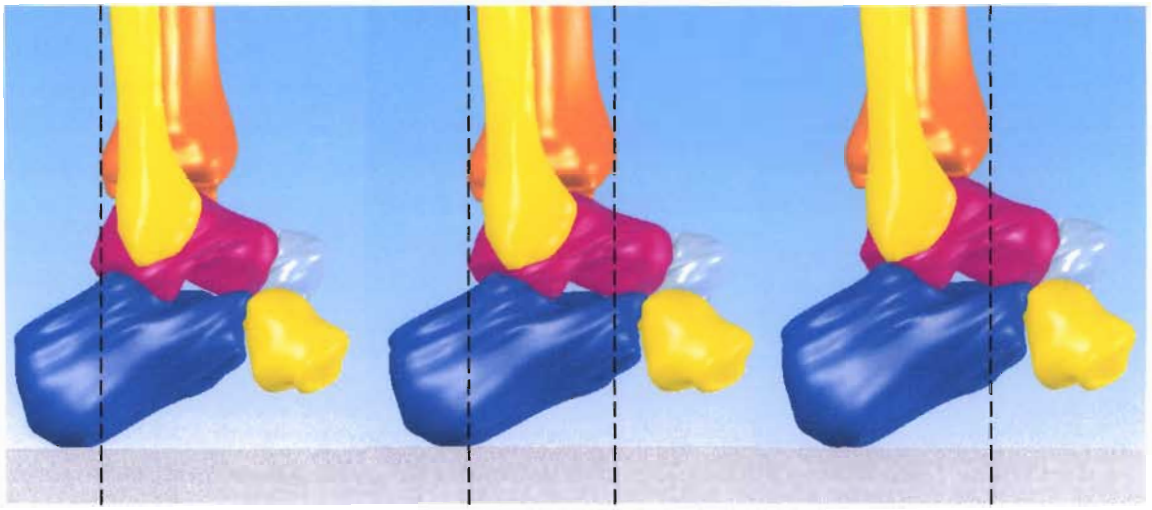

Figure 5.3.6: Bony Movement of the Ankle Complex- ATFL+CFL Suppressed Configuration: Foot on the left represents the positioning after application of the posterior force, foot in the center represent the starting position, and foot on the right represents positioning after the application of the anterior force. Notice the slight increase in posterior movement of the talus and calcaneus with respect to the tibia from Figure 5.3.5.

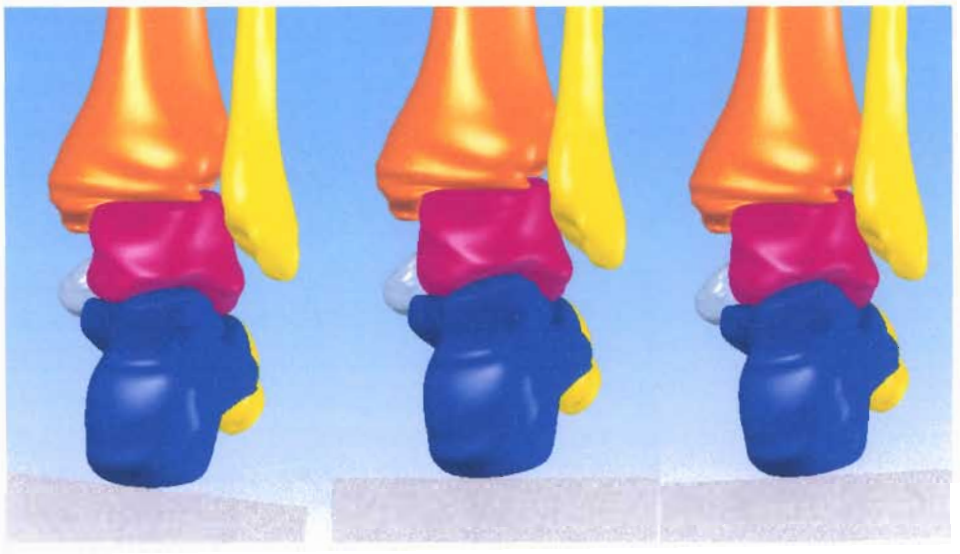

Figure 5.3.7: Bony Movement of the Ankle Complex- Intact Configuration: Foot on the left represents the positioning after the application of the inversion force, foot in the center represent the starting position, and foot on the right represents positioning after the application of the eversion force. Notice how the inversion and eversion movement occurs correctly between the talus and calcaneus.

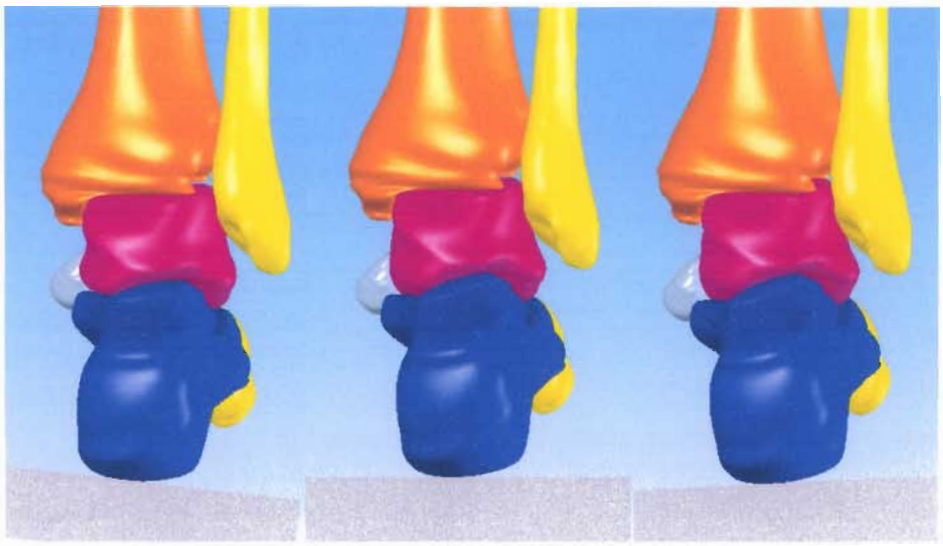

Figure 5.3.8: Bony Movement of the Ankle Complex- ATFL Suppressed Configuration: Foot on the left represents the positioning after the application of the inversion force, foot in the center represent the starting position, and foot on the right represents positioning after the application of the eversion force. Notice how the inversion and eversion movement occurs correctly between the talus and calcaneus. The minimal differences that occur cannot be distinguished from the previous figure (Figure 5.3.7).

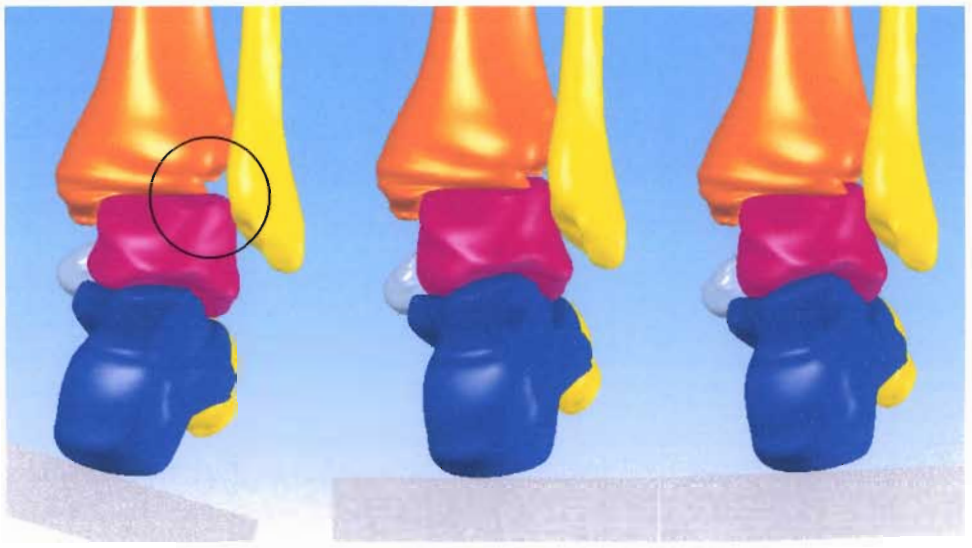

Figure 5.3.9: Bony Movement of the Ankle Complex- ATFL Suppressed Configuration: Foot on the left represents the positioning after the application of the inversion force, foot in the center represent the starting position, and foot on the right represents positioning after the application of the eversion force. Notice the excessive movement of the talus and the gapping in between the tibia and talus (circled). This gapping is an indication of a torn calcaneofibular ligament.

Additional information may be garnered from this computational model that cannot be readily measured experimentally. In the anterior/posterior simulation, under the application of the anterior force, several ligaments displayed minor changes in force after the suppression of the ATFL, (Table 5.3.1) suggesting the bony architecture plays major role in resisting anterior translation with a transected ATFL. In the anterior/posterior simulation, under the application of the posterior force, the CFL displayed an increase of 16N after the suppression of the ATFL and the posterior

tibiotalar ligament saw an increase of 33N with the suppression of the ATFL and CFL. (Table 5.3.2) Most notable to mention in the inversion/eversion simulation, under the application of the inversion torque, the anterior tibiofibular (distal), lateral talocalcaneal, posterior talofibular, and posterior tibiofibular (distal) ligaments' force all increased by over 25N with the suppression of the CFL. (Table 5.3.3) These ligaments along with the bony architecture are the restricting factors. Also in the inversion/eversion simulation under the application of the eversion torque, the tibiocalcaneal and posterior tibiofibular (distal) ligaments all decreased by at least 15N after suppression of the CFL. (Table 5.3.4)

Contact forces were recorded between the talus and tibia, calcaneus and talus, talus and fibula, and talus and navicular. A reduction in force was seen between the talus and fibula, under application of the anterior force, after suppression of the ATFL. (Table 5.3.5) A reduction in force was seen between the talus and fibula, under application of the posterior force, after suppression of the CFL. (Table 5.3.6) Reductions in force were seen between the talus and tibia, and the calcaneus and talus, under application of the inversion and eversion moments, after suppression of the CFL. (Table 5.3.7 & 5.3.8)

Ligaments	Approximate Force (N) in Major Ligaments Elongating and Resisting Anterior Force		
	Intact	**ATFL Transected**	**ATFL+CFL Transected**
Anterior talofibular	40	--	--
Anterior tibiofibular (distal)	40	45	45
Anterior tibiotalar	93	94	94
Dorsal talonavicular 2	77	71	71
Lateral talocalcaneal	48	38	37
Posterior tibiofibular (distal)	50	34	35
Tibiocalcaneal	93	100	100
Tibionavicular	96	105	105

Table 5.3.2: Ligament Forces- Laxity Study (Anterior Force): The magnitude of load seen in the major springs (ligaments) resisting movement during the anterior force configurations. Several ligaments displayed changes in force after the transection of the ATFL. The posterior tibiofibular ligament displayed the largest change, a 16N decrease.

Ligaments	Approximate Force (N) in Major Ligaments Elongating and Resisting Posterior Force		
	Intact	**ATFL Transected**	**ATFL+CFL Transected**
Calcaneofibular	70	86	--
Dorsal Talonavicular 2	60	63	80
Posterior tibiofibular (distal)	45	35	33
Posterior tibiotalar	120	117	150
Tibiocalcaneal	50	46	60

Table 5.3.3: Ligament Forces- Laxity Study (Posterior Force): The magnitude of load seen in the major springs (ligaments) resisting movement during the posterior force configurations. When the ATFL was suppressed, the force of the calcaneofibular ligament increased. After the ATFL and CFL ligaments were suppressed, the force of the tibotalar ligament greatly increased.

Ligaments	Approximate Force (N) in Major Ligaments Elongating and Resisting Inversion Moment		
	Intact	**ATFL Transected**	**ATFL+CFL Transected**
Calcaneofibular	165	168	--
Anterior tibiofibular (Distal)	74	74	100
Dorsal talonavicular 2	116	105	90
Lateral talocalcaneal	120	108	170
Posterior talofibular	12	12	134
Posterior tibiofibular (distal)	55	40	90

Table 5.3.4: Ligament Forces- Laxity Study (Inversion Moment): The magnitude of load seen in the major springs (ligaments) resisting movement during the inversion force configurations. When the ATFL and CFL were suppressed the force of many ligaments greatly increased.

Ligaments	Approximate Force (N) in Major Ligaments Elongating and Resisting Eversion Moment		
	Intact	**ATFL Transected**	**ATFL+CFL Transected**
Anterior tibiotalar	48	49	40
Medial talocalcaneal	20	25	28
Posterior talocalcaneal	17	20	25
Posterior tibiofibular (distal)	33	20	6
Tibiocalcaneal	153	153	135
Tibionavicular	38	39	20

Table 5.3.5: Ligament Forces- Laxity Study (Eversion Moment): The magnitude of load seen in the major springs (ligaments) resisting movement during the eversion force configurations: When the ATFL and CFL ligaments were suppressed, the force of many ligaments reduced.

Bony Contacts	Approximate Magnitude of Contact Force (N) During Anterior Force		
	Intact	ATFL Transected	ATFL+CFL Transected
Talus and tibia	255	270	270
Calcaneus and talus	240	235	245
Talus and fibula	40	25	30
Talus and navicular	100	100	100

Table 5.3.6: Contact Forces- Laxity Study (Anterior Force): The magnitude of the contact forces seen in the major articulations of the foot/ankle complex for the anterior force configurations. Notice the reduction in contact force between the talus and fibula, and the increase in contact force between the talus and tibia after the ATFL is transected.

Bony Contacts	Approximate Magnitude of Contact Force (N) During Posterior Force		
	Intact	ATFL Transected	ATFL+CFL Transected
Talus and tibia	240	225	210
Calcaneus and talus	80	90	60
Talus and fibula	105	95	45
Talus and navicular	260	277	255

Table 5.3.7: Contact Forces- Laxity Study (Posterior Force): The magnitude of the contact forces seen in the major articulations of the foot/ankle complex for the posterior force configurations. The contact force was greatly reduced between the talus and fibula with transection of the ATFL and CFL ligaments.

Bony Contacts	Approximate Magnitude of Contact Force (N) During Inversion Moment		
	Intact	ATFL Transected	ATFL+CFL Transected
Talus and tibia	225	225	175
Calcaneus and talus	300	300	200
Talus and fibula	200	180	175
Talus and navicular	275	275	125

Table 5.3.8: Contact Forces- Laxity Study (Inversion Moment): The magnitude of the contact forces seen in the major articulations of the foot/ankle complex for the inversion force configurations. The contact forces greatly reduced between the talus and tibia, calcaneus and talus, and talus and navicular with transection of the ATFL and CFL ligaments.

Bony Contacts	Approximate Magnitude of Contact Force (N) During Eversion Moment		
	Intact	ATFL Transected	ATFL+CFL Transected
Talus and tibia	275	275	175
Calcaneus and talus	200	200	175
Talus and fibula	50	45	50
Talus and navicular	150	170	130

Table 5.3.9: Contact Forces- Laxity Study (Eversion Moment): The magnitude of the contact forces seen in the major articulations of the foot/ankle complex for the eversion force configurations. The contact force between the talus and tibia is greatly reduced with transection of the ATFL and CFL ligaments.

5.4 ADDITION COMPARISON: CADAVER ANTERIOR DRAWER TEST

For an additional comparison, especially to ligament elongation, an additional cadaver anterior drawer test was performed in our laboratory. One fresh, frozen cadaver lower leg without evidence of injury to any ligaments that would affect anterior movement as within the ankle complex was used for this study. A section of skin was dissected from the lateral surface of the ankle in order to expose the anterior talofibular ligament (ATFL) and the calcaneofibular ligament (CFL).

The specimen was mounted to the foot plate and then attached to the actuator of the mechanical testing machine. The tibia rested on a tibial plate, which was fixed to the base of the Instron via an XY translator and a three axis vice (Figure 6.2.1). The foot of the specimen was placed onto the footplate with a #10 woodscrew inserted through the heel plate into the posterior aspect of the calcaneus. A ladder strap with buckle was placed over the midfoot and tightened to secure/fix the midfoot and forefoot to the footplate. Woodscrews were used to fix the lower leg to the tibial plate. The loading of the specimen into the design setup can be seen in the figures below.

Figure 5.4.1: Cadaveric Foot Mounted in the Testing Jig: The tibia plate held the lower leg in place. The calcaneus is screwed into the heel plate. The forefoot and midfoot were held by two sliding mechanisms and a locking strap. The DVRT is seen as the white cable leaving the dissected area.

In the Anterior Drawer test, the footplate was positioned such that the lower leg was fixed in its neutral position (0 degrees dorsiflexion and plantar flexion). The footplate was then locked into position using the multi-axial hardware. Neutral position can be defined as when the foot is neither pronated or supinated, and the sagittal plane bisector of the calcaneus is at 90 degrees to the supporting surface.[49] Two calibrated differential variable reluctance transducers (DVRT's; Microstrain, Williston, VT) were inserted into the ATFL and the CFL. Using stroke control, the materials testing machine was programmed to produce an 8 or 9.25mm crosshead movement in an upward direction

to simulate the Anterior Drawer test, for intact and cut ATFL respectively. Three tests were conducted for the each specimen configuration (intact, transected ATFL). Each test consisted of the crosshead moving in a continuous cyclic loading and unloading pattern for ten cycles at a rate of four seconds per cycle at a rate of 4mm/sec. Force and position data were recorded for the cross head motion as well as the load cell response within the mechanical testing machine at a rate of 10 Hz. Voltage corresponding to position data was recorded for each of the DVRTs at 10 Hz. Specimens were given 90 seconds between tests to allow soft tissue equilibration. After three tests were conducted for the intact specimen, the ATFL DVRT was removed, and the ATFL was transected to simulate deficiency in the ATFL due to injury. The cyclic process was repeated three times for the deficient specimen and the results recorded.

The results obtained from the cadaveric foot are as follows. The difference in displacement from intact to cut ATFL was 1.25mm to reach a comparable load study conducted by Kovaleski.[44] The DVRT in the ATFL indicated approximately 0.5mm of displacement for the ATFL in the intact configuration. The CFL length remained relatively constant in the intact and transected configurations.

In the corresponding computational simulation (anterior portion of anteroposterior laxity test), the anterior tibiofibular ligament elongation was found to be 0.455mm. In both simulations, intact and transected, the CFL did not elongate. Anterior Displacement increased by 0.3mm with the transection of the ATFL.

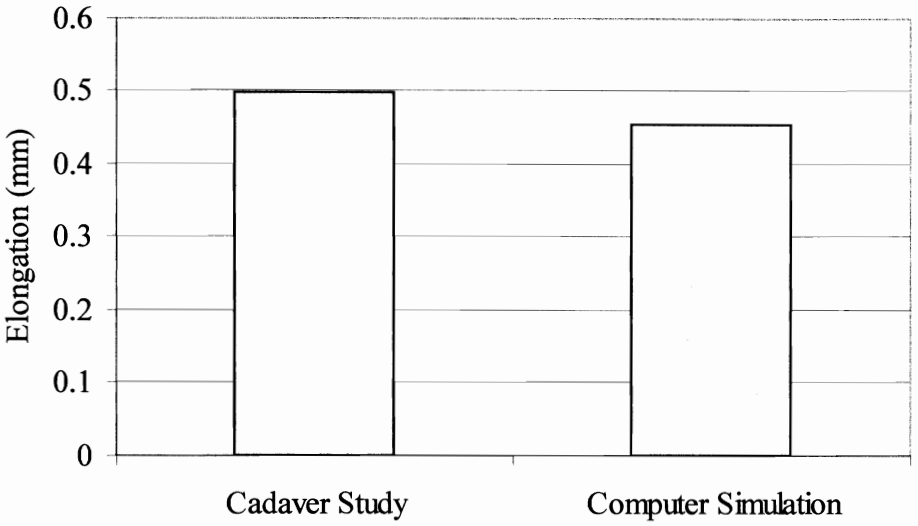

Figure 5.4.2: ATFL Elongation in the Cadaver Study and Computational Model: Similar elongation occurred in the anterior talofibular ligament in the cadaver foot and anterior portion of the computational simulation. There is a difference of only 9% when compared to the experimental data.

5.5 DISCUSSION

The present computational simulations of anterior/posterior and inversion/eversion laxity of the foot revealed a capability to predict differences in joint kinematics with varying ligament deficiencies. In the anterior/posterior part of this study, all three models predicted anterior/posterior laxity within the standard deviations of the cadaver study. The correct trend was seen after the transaction of each ligament. After the transaction of the ATFL, the additional movement occurred in the anterior and posterior directions, and after the transection of the CFL, the majority of the additional movement occurred in the posterior direction. This corresponds to the physiological role

the ATFL has to restrict forward movement of the talus with respect to the tibia and the CFL to restrict posterior movement of the calcaneus with respect to the tibia.

In inversion/eversion, no difference was seen between intact and transected ATFL states; however, a major increase in inversion was seen after the transaction of the CFL. The CFL is the main ligament preventing inversion, and a change was expected. In a similar fashion to the Ankle Inversion Stability, gapping was seen between the talus and tibia after transection of the CFL. Absolute values differed slightly from that of cadaver study. Another cadaver study showed differences of less then 1mm and greater than 10 degrees in supination (closely identical to inversion axis seen in the comparative study), when loading to 5.7N-m, after the transections of the ATFL and ATFL+CFL, respectively.[48]

The computational model of the Anterior portion of the anteroposterior laxity test, did show a difference between healthy and ligament deficient ankles. Magnitudes of anterior displacement seen in the computational study were far less than those seen in the cadaver foot. In the cadaver foot tested in our laboratory, the DVRT data for the anterior talofibular ligament showed similar elongation results when compared to the anterior simulation.

Many studies have focused on just the Anterior Drawer test and have varying results. Several studies used actual patients with unilateral ankle sprains. One patient study showed a displacement of approximately 12 and 17mm for healthy and injured ankles, respectively, when loaded to the corresponding values of this study.[27] In another patient study, using stress radiography and loading to 147N, healthy ankles were

seen to have a displacement of 1.7±1.3mm in their control group and 8.9±4.3mm after ankle sprain.[50] Another study, loading to 125N, using stress radiographic measurements found uninjured ankles to have displacements of 6.2±2.2mm and ankles with functional instability to have displacements of 6.9±2.5mm.[51] A cadaver study conducted by Kerkhoffs et al. showed differences of 2.0 and 2.7mm in the anterior direction, when loading to 150N, after the transections of the ATFL and ATFL+CFL; however, this study was not measuring bony motion and the foot was in a position of 15 degrees plantar flexion.[47] Another cadaver study showed differences of less than 1mm and greater than 3.5mm in the anterior direction, when loading to 80N, after the transections of the ATFL and ATFL+CFL, respectively. This study also used buckle transducers to measure the force present in the ATFL and CFL during the test. The force measured by the buckle transducer was approximately 23N for the ATFL and 15N for the CFL.[48] At a load of 80N, the computational simulation predicted a load of 27.5N present in the ATFL. One cadaveric study looked at the Anterior Drawer test when the foot was loaded between 10 and 50N. The anterior displacements seen were approximately 2.25mm for both intact and transected ATFL, and showed the displacement starting to level out after 50N.[52] It must be mentioned that fixation of the bones in the cadaveric experimental study is far superior to how well the bones can be held in place in a patient studies, this in turn creates the possibility of more soft tissue movement/displacement. Still the only truly accurate way to measure bony displacement is to track the bones directly either with a spatial kinematic linkage system, radiographs, or other methods.

Differences that should be noted between the computer simulation and cadaver study are: simulation modeled a particular foot whereas the cadaver study included 6 feet; ligaments were represented as a linear springs with an in situ strain displacing each ligament beyond its toe region; bony architecture was partially dependent upon surface fitting techniques within computer programs; and ligament stiffness and placement were controlled by the simulator. Also all bones were viewed as rigid that could not deform. Midfoot and forefoot were grouped together as one rigid body. In the cadaver tests, the midfoot and forefoot were clamped/strapped down tightly, however they may still have a slight ability to move. Since the measurement in this cadaver study is of the bony motion, soft tissue movement is less of a factor, therefore, making this comparison very meaningful.

CHAPTER 6: OVERALL DISCUSSION

Computational models of musculoskeletal joints and limbs can provide useful information about joint mechanics. This model of the lower leg has been compared to three previously performed cadaver studies (syndesmotic injury study, inversion stability study, and mechanical laxity study) and one simultaneously performed study (anterior drawer study). These studies were used to validate the models and methods created in this dissertation. The overall goal of creating these computational models is for them to eventually be used as a predictive device for understanding joint function and serve as a clinical tool for predicting the outcome of surgical procedures. This new modeling approach simulates joint kinematics dictated by bone/joint anatomy, ligamentous constraints, and applied loading.

The development of these computational models began with the use of MIMICS in the generation of three-dimensional surfaces from CT images, followed by importing these surfaces into SolidWorks and COSMOSMotion. Through SolidWorks and COSMOSMotion, each bone surface was created into a solid object and positioned, necessary components added, and simulations executed. Three dimensional contacts inhibited intersection of the bones during motion. Ligaments were represented as linear springs. As for the deformation of the bones and of the cartilage layers, Walker et al.

1972, stated these deformations can be ignored because of the fact that they are relatively small when compared to the displacements of the joints.[53] The rational for ignoring friction in these simulation came from Radin et al., another investigator in the earlier seventies, who mentioned friction is very low due to the presence of cartilage surfaces and the synovial fluid.[54] Density of each part is not a major variable, due to the fact every moving object has an identical density and the bony geometry and ligaments are the major constraints in each simulation. To prove this point, simulations were run while varying the densities of parts, and no difference in results was seen. A major advantage of this modeling technique is that it may be performed in any laboratory through the use of several commercially available programs.

Some limitations still exist with these modeling procedures, however, it may be possible to resolve these limitations by working with the software companies, and using additional individual, specimen specific data. The first major limitation is the time consuming process of making a three-dimensional model of an individual foot. This study used only one particular foot to model, as a representative foot for an entire population. Ideally, it would be beneficial to have an automated process to produce the individual architecture of each foot, however this system would still be partially dependent on curve fitting techniques and could still possible create slight variations in surface geometries. Also if MRI images were taken, more precise placement of each ligament may be incorporated, thus producing the exact line(s) of action of each ligamentous constraint. The difference in the linearity of the springs could be resolved through communication with COSMOSMotion to achieve tension only springs, where the

user can control the governing stiffness equation. The stiffness and preloading values of each ligament is a more difficult complication. It must be noted that stiffness and preload values can vary between specimen according to sex, size, weight, gender, etc. Upon further investigation, the hope would be that a representative stiffness and preload value would be adequate in predicting differences. In our simulations, preload values were incorporated not only because they are present in normal stance, but it also prevents the springs from entering into a compressive state. Differences in motion due to changes in stiffness values have been analyzed in both and Chapters 3 and 4. With an addition of tension only, non-linear springs, the preload values may have less of an effect, and a greater magnitude of motion could possibly be seen. In some simulations, multiple bones were viewed as one rigid object. This assumption was made to reduce the computational power needed to analyze the model. With the progression of computers and software used to analyze dynamic motion, this assumption could be reduced or eliminated. Also in cadaveric foot studies, there will always be varying amounts of soft tissue movements, and/or movements due to give within the loading and fixation jigs. We saw in the present results that the magnitudes of the results were closer in magnitude to those studies measuring bony movements (Chapters 4 and 5).

Our computational model had success in demonstrating differences seen in every cadaver study, even if some results were not as comparable in magnitude. The syndesmotic injury model was able to predict differences in tibial rotation, fibular rotation, and anterior/posterior displacement. In the inversion simulation, calcaneofibular ligament extension and angles of inversion compared well. The laxity study showed

increases in anteroposterior motion after the transactions of the ATFL and CFL; and differences in inversion after the transection of the CFL. The Anterior Drawer simulation (anterior part of anteroposterior laxity study) produced similar ligament elongations and loads when compared to a cadaver test.

Overall, the computational models were able to predict joint kinematics of the lower leg with particular focus on the ankle complex. Additional parameters can be calculated through such models that are not easily obtained experimentally such as ligament forces, force transmission across joints, and three-dimensional movement of all bones. Through future investigation this type of computational model could be of great value to the medical community.

REFERENCES

REFERENCES

1. Delp, S.L. and J.P. Loan, *A graphics-based software system to develop and analyze models of musculoskeletal structures.* Comput Biol Med, 1995. **25**(1): p. 21-34.

2. Piazza, S.J. and S.L. Delp, *Three-dimensional dynamic simulation of total knee replacement motion during a step-up task.* J Biomech Eng, 2001. **123**(6): p. 599-606.

3. Chao, E.Y., *Graphic-based musculoskeletal model for biomechanical analyses and animation.* Med Eng Phys, 2003. **25**(3): p. 201-12.

4. Delp, S.L., et al., *An interactive graphics-based model of the lower extremity to study orthopaedic surgical procedures.* IEEE Trans Biomed Eng, 1990. **37**(8): p. 757-67.

5. Chao, E.Y., J.D. Lynch, and M.J. Vanderploeg, *Simulation and animation of musculoskeletal joint system.* J Biomech Eng, 1993. **115**(4B): p. 562-8.

6. Holzbaur, K.R., W.M. Murray, and S.L. Delp, *A model of the upper extremity for simulating musculoskeletal surgery and analyzing neuromuscular control.* Ann Biomed Eng, 2005. **33**(6): p. 829-40.

7. Buford, W., L. Meyers, and A. Hollister, *Modeling Simulation System for the Human Hand.* Journal of Clinical Engineering, 1990. **15**: p. 445-451.

8. Delp, S.L., K. Statler, and N.C. Carroll, *Preserving plantar flexion strength after surgical treatment for contracture of the triceps surae: a computer simulation study.* J Orthop Res, 1995. **13**(1): p. 96-104.

9. Cheung, J.T., K.N. An, and M. Zhang, *Consequences of partial and total plantar fascia release: a finite element study.* Foot Ankle Int, 2006. **27**(2): p. 125-32.

10. Cheung, J.T., et al., *Three-dimensional finite element analysis of the foot during standing--a material sensitivity study.* J Biomech, 2005. **38**(5): p. 1045-54.

11. Reggiani, B., et al., *Finite element analysis of a total ankle replacement during the stance phase of gait.* J Biomech, 2006. **39**(8): p. 1435-1443.

12. Kwak, S.D., L. Blankevoort, and G.A. Ateshian, *A Mathematical Formulation for 3D Quasi-Static Multibody Models of Diarthrodial Joints.* Comput Methods Biomech Biomed Engin, 2000. **3**(1): p. 41-64.

13. Wismans, J., et al., *A three-dimensional mathematical model of the knee-joint.* J Biomech, 1980. **13**(8): p. 677-85.

14. Hirokawa, S., *Three-dimensional mathematical model analysis of the patellofemoral joint.* J Biomech, 1991. **24**(8): p. 659-71.

15. Gonzalez, R.V., T.S. Buchanan, and S.L. Delp, *How muscle architecture and moment arms affect wrist flexion-extension moments.* J Biomech, 1997. **30(7): p.** 705-12.

16. Arnold, A.S., S.S. Blemker, and S.L. Delp, *Evaluation of a deformable musculoskeletal model for estimating muscle-tendon lengths during crouch gait.* Ann Biomed Eng, 2001. **29**(3): p. 263-74.

17. Yoshida, H., et al., *Three-dimensional dynamic hip contact area and pressure distribution during activities of daily living.* J Biomech, 2005.

18. Lin, H.T., et al., *Use of virtual, interactive, musculoskeletal system (VIMS) in modeling and analysis of shoulder throwing activity.* J Biomech Eng, 2005. **127**(3): p. 525-30.

19. Goldsworthy, J., et al., *Acheivving Physiologic Rotation in Patient-Specific Contact Stress Analysis of the Ankle*, in *52nd Annual Meeting: Orthopaedic Research Society*. 2006: Chicago, IL.

20. de Asla, R.J., et al., *Six DOF in vivo kinematics of the ankle joint complex: Application of a combined dual-orthogonal fluoroscopic and magnetic resonance imaging technique.* J Orthop Res, 2006. **24**(5): p. 1019-27.

21. Siegler, S., et al., *Mechanics of the ankle and subtalar joints revealed through a 3D quasi-static stress MRI technique.* J Biomech, 2005. **38**(3): p. 567-78.

22. Li, G., et al. *Reciprocal Function of Anterior Talofibular and Calcaneofibular Ligaments During In-Vivo Motion of the Ankle Joint Complex.* in *52nd Annual Meeting: Orthopaedic Research Society*. 2006. Chicago, IL.

23. Ringleb, S.I., et al., *The effect of ankle ligament damage and surgical reconstructions on the mechanics of the ankle and subtalar joints revealed by three-dimensional stress MRI.* J Orthop Res, 2005. **23**(4): p. 743-9.

24. Kapit, W. and L.M. Elson, *The anatomy coloring book.* 3rd ed. 2002, San Francisco: Benjamin Cummings. 1 v. (various pagings).

25. Levangie, P.K. and C.C. Norkin, *Joint structure and function: a comprehensive analysis*. 3rd. ed. 2001, Philadelpha: F.A. Davis.

26. Nyska, M. and G. Mann, *The unstable ankle*. 2002, Champaign, IL: Human Kinetics. xv, 319.

27. Liu, W., S. Siegler, and L. Techner, *Quantitative measurement of ankle passive flexibility using an arthrometer on sprained ankles.* Clin Biomech (Bristol, Avon), 2001. **16**(3): p. 237-44.

28. Hoppenfeld, S. and R. Hutton, *Physical examination of the spine and extremities.* 1976, New York: Appleton-Century-Crofts. xi, 276.

29. *Mimics: Reference Guide*. Vol. Version 7.3: Materialise Software.

30. Netter, F.H. and J.T. Hansen, *Atlas of human anatomy*. 3rd ed. 2003, Teterboro, N.J.: Icon Learning Systems. 542 p. of plates, [53].

31. Agur, A.M.R., M.J. Lee, and J.C.B. Grant, *Grant's atlas of anatomy*. 10th ed. 1999, Philadelphia: Lippincott Williams & Wilkins. XVI, 760.

32. *COSMOSMotion User's Guide.* 2002.

33. Attarian, D.E., et al., *Biomechanical characteristics of human ankle ligaments.* Foot Ankle, 1985. **6**(2): p. 54-8.

34. Beumer, A., et al., *A biomechanical evaluation of the tibiofibular and tibiotalar ligaments of the ankle.* Foot Ankle Int, 2003. **24**(5): p. 426-9.

35. Siegler, S., J. Block, and C.D. Schneck, *The mechanical characteristics of the collateral ligaments of the human ankle joint.* Foot Ankle, 1988. **8**(5): p. 234-42.

36. Pfaeffle, H.J., et al., *Tensile properties of the interosseous membrane of the human forearm.* J Orthop Res, 1996. **14**(5): p. 842-5.

37. Woo, S.L., et al., *Measurement of changes in ligament tension with knee motion and skeletal maturation.* J Biomech Eng, 1990. **112**(1): p. 46-51.

38. Blankevoort, L. and R. Huiskes, *Ligament-bone interaction in a three-dimensional model of the knee.* J Biomech Eng, 1991. **113**(3): p. 263-9.

39. Blankevoort, L., et al., *Articular contact in a three-dimensional model of the knee.* J Biomech, 1991. **24**(11): p. 1019-31.

40. Marqueen, T., et al., *Comparison of the syndesmotic staple to the transsyndesmotic screw: a biomechanical study.* Foot Ankle Int, 2005. **26**(3): p. 224-30.

41. Fung, Y.C., *Biomechanics: mechanical properties of living tissues*. 2nd ed. 1993, New York: Springer-Verlag. xviii, 568 p.

42. Martin, L.P., et al., *Elongation behavior of calcaneofibular and cervical ligaments during inversion loads applied in an open kinetic chain.* Foot Ankle Int, 1998. **19**(4): p. 232-9.

43. Kjaersgaard-Andersen, P., J.O. Wethelund, and S. Nielsen, *Lateral talocalcaneal instability following section of the calcaneofibular ligament: a kinesiologic study.* Foot Ankle, 1987. **7**(6): p. 355-61.

44. Kovaleski, J.E., et al., *Assessment of Ankle-Subtalar-Joint-Complex Laxity Using an Instrumented Ankle Arthrometer: An Experimental Cadaveric Investigation.* J Athl Train, 2002. **37**(4): p. 467-474.

45. Kovaleski, J.E., et al., *Instrumented measurement of anteroposterior and inversion-eversion laxity of the normal ankle joint complex.* Foot Ankle Int, 1999. **20**(12): p. 808-14.

46. Kerkhoffs, G.M., et al., *An instrumented, dynamic test for anterior laxity of the ankle joint complex.* J Biomech, 2002. **35**(12): p. 1665-70.

47. Kerkhoffs, G.M., L. Blankevoort, and C.N. van Dijk, *A measurement device for anterior laxity of the ankle joint complex.* Clin Biomech (Bristol, Avon), 2005. **20**(2): p. 218-22.

48. Bahr, R., et al., *Mechanics of the anterior drawer and talar tilt tests. A cadaveric study of lateral ligament injuries of the ankle.* Acta Orthop Scand, 1997. **68**(5): p. 435-41.

49. Rockar, P.A., Jr., *The subtalar joint: anatomy and joint motion.* J Orthop Sports Phys Ther, 1995. **21**(6): p. 361-72.

50. Spahn, G., *The ankle meter: an instrument for evaluation of anterior talar drawer in ankle sprain.* Knee Surg Sports Traumatol Arthrosc, 2004. **12**(4): p. 338-42.

51. Hubbard, T.J., et al., *Quantitative assessment of mechanical laxity in the functionally unstable ankle.* Med Sci Sports Exerc, 2004. **36**(5): p. 760-6.

52. Tohyama, H., et al., *Biomechanical analysis of the ankle anterior drawer test for anterior talofibular ligament injuries.* J Orthop Res, 1995. **13**(4): p. 609-14.

53. Walker, P.S. and J.V. Hajek, *The load-bearing area in the knee joint.* J Biomech, 1972. **5**(6): p. 581-9.

54. Radin, E.L. and I.L. Paul, *A consolidated concept of joint lubrication.* J Bone Joint Surg Am, 1972. **54**(3): p. 607-13.

ACKNOWLEDGEMENT

The CT datasets were provided by: